Available online at www.sciencedirect.com
ScienceDirect
Ocean Engineering 34 (2007) 1650–1667
OCEAN ENGINEERING
www.elsevier.com/locate/oceaneng

Planar trajectory planning and tracking control design for underactuated AUVs

Filoktimon Repoulias, Evangelos Papadopoulos*

Department of Mechanical Engineering, National Technical University of Athens, 15780 Athens, Greece

Received 16 May 2006; accepted 1 November 2006
Available online 12 February 2007

Abstract

This paper addresses the combined problem of trajectory planning and tracking control for underactuated autonomous underwater vehicles (AUVs) on the horizontal plane. Given a smooth, inertial, 2D reference trajectory, the planning algorithm uses vehicle dynamics to compute the reference orientation and body-fixed velocities. Using these, the error dynamics are obtained. These are stabilized using backstepping techniques, forcing the tracking error to an arbitrarily small neighborhood of zero. Simulation results for a constant velocity trajectory, i.e. a circle, and a time-varying velocity one, i.e. a sinusoidal path, are presented. The parametric robustness is considered and it is shown that tracking remains satisfactory.

Keywords: Underactuated AUV; Trajectory planning; Tracking control

1. Introduction

Over the past two decades, a great amount of research has been conducted regarding the operation of autonomous underwater vehicles (AUVs), see Fig. 1. AUVs are playing a crucial role in exploration and exploitation of resources located at deep oceanic environments. They are employed in risky missions such as oceanographic observations, bathymetric surveys, ocean floor analysis, military applications, recovery of lost man-made objects, etc. (Yuh, 2000). Besides their numerous practical applications, AUVs present a challenging control problem since most of them are underactuated, i.e., they have fewer actuated inputs than degrees of freedom (DOF), imposing nonintegrable acceleration constraints. In addition, AUVs' kinematic and dynamic models are highly nonlinear and coupled (Fossen, 1994), making control design a hard task. Underactuation rules out the use of trivial control schemes, e.g., full state-feedback linearization (Khalil, 1996), and the complex hydrodynamics excludes designs based on the kinematic model only. Note that when moving on a horizontal plane, AUVs present similar dynamic behavior to underactuated surface vessels (Aguiar and Pascoal, 2002; Fossen, 1994).

The planar stabilization problem for surface vessels and AUVs, i.e., regulation to a point with a desired orientation, has been studied by various researchers; see for example (Aguiar and Pascoal, 2002; Wichlund et al., 1995; Reyhanoglou, 1997; Pettersen and Egeland, 1999; Pettersen and Fossen, 2000; Mazenc et al., 2002). In these works, it is shown that such vehicles cannot be asymptotically stabilized by continuous time-invariant feedback control laws.

Trajectory tracking requires the design of control laws that guide the vehicle to track an inertial reference trajectory, i.e., a geometric path on which a time law is specified. Existing tracking controller designs for underactuated marine vehicles in use—AUVs and surface vessels—follow classical approaches such as local linearization and decoupling of the multivariable model to steer as many DOF as the available control inputs. According to this methodology, the six DOF vehicle is decoupled into two reduced dynamical systems: a depth—pitch model that considers motion in the vertical plane and a plane—yaw model that studies the motion in the horizontal plane.

*Corresponding author. Fax: +30 210 772 1455.
E-mail address: egpapado@central.ntua.gr (E. Papadopoulos).

0029-8018/$ - see front matter © 2007 Elsevier Ltd. All rights reserved.
doi:10.1016/j.oceaneng.2006.11.007

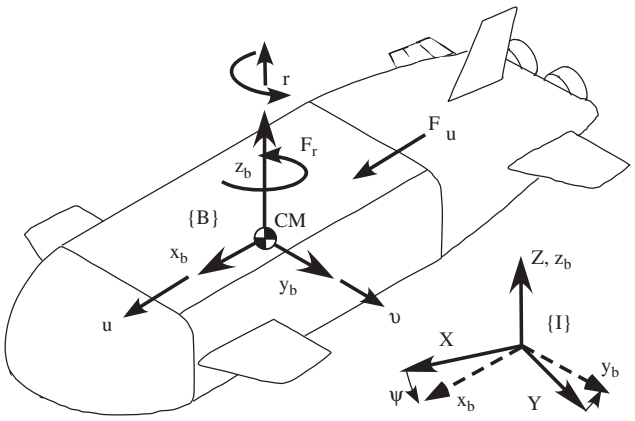

Fig. 1. The underactuated AUV model in plane motion.

The two resulting models are then linearized around a constant nominal forward velocity. Control design is carried out using standard linear (or nonlinear) methods, see (Fossen, 1994). Other approaches include the linearization of the vehicle's error dynamics about "trimming" trajectories—tracking with constant required velocities—that lead to time-invariant linear systems followed by such techniques as gain scheduling, see (Kaminer et al., 1998). The validity of these solutions is limited in a small neighborhood around the selected operating points. Stability and performance also suffer significantly when the vehicle executes maneuvers that excite the effects of its complex hydrodynamics and nonlinear coupling terms.

On the other hand, theoretical and experimental results on trajectory tracking for autonomous underactuated marine vehicles show that nonlinear Lyapunov-based techniques can overcome most of the limitations mentioned above. The authors in Pettersen and Nijmeijer (2001) and Lefeber et al. (2003), present experimental tracking results for a model surface ship using Lyapunov-based controllers. In Jiang (2002), two tracking solutions for a surface vessel were proposed, based on Lyapunov's direct method and passivity approach. However, in the last three works, the yaw velocity is required to be nonzero; under this restriction straight lines cannot be tracked. Also, the drag force model, i.e., the rigid body resistance as it moves through the water is assumed to be a linear function with respect to the velocity in all three DOF motion. This means that the results are valid only when the vehicle moves with low velocities. In Behal et al. (2002), the error dynamics is transformed into a skew-symmetric form and practical convergence is achieved; the authors also consider a linear drag force model. The authors in Aguiar and Hespanha (2003), have designed a controller for marine vehicles moving in two or three dimensions that exponentially forces the position tracking error to a small neighborhood of the origin. However, the attitude is left uncontrolled which may result in position tracking with undesirable attitude. The stabilization of the velocities error is not mentioned as well; this is an equally important matter since even in the case of exact position tracking, large velocity errors may lead to actuator saturation. In Repoulias and Papadopoulos (2005), a trajectory planning and a tracking-control algorithm for an underactuated AUV moving on the horizontal plane were studied. The model of drag force used was linear with respect to velocities; also the planning algorithm was applied for a plane circular trajectory that required constant tracking velocities from the AUV.

In this paper, the combined problem of trajectory planning and tracking control for underactuated AUVs moving on the horizontal plane—constant depth motion—is addressed. The goal of trajectory planning is to generate feasible reference inputs to the motion control system which in turn ensures that the vehicle executes the planned trajectory. Given a smooth 2D reference inertial trajectory, the planning algorithm produces the corresponding reference body-fixed linear and angular velocities and accelerations, as well as the reference orientation. The algorithm is based on the dynamics of the AUV rendering the body-fixed reference trajectory feasible. The trajectories used for the illustration of the method are a circle with constant body-fixed velocities and a sinusoidal curve, which requires time-varying body velocities, i.e., nonzero accelerations. In addition, the drag forces in all three DOF of motion are quadratic with respect to the velocities. Using the resulting reference variables, the vehicle error dynamics is obtained and the control problem reduces to an error dynamics stabilization problem. To this end, methods such as partial state-feedback linearization, backstepping, and nonlinear damping are used to design a time-varying closed-loop trajectory-tracking control law which forces the tracking errors to a neighborhood of zero that can be reduced arbitrarily. A natural requirement in the above procedure is that the surge velocity is nonzero. The robustness in the presence of parameter uncertainty is also studied and the results show that tracking remains very satisfactory. Simulation results that demonstrate the performance of the developed control design are presented and discussed.

2. AUV kinematics and dynamics

In this section, the kinematic and dynamic equations of the motion of an AUV moving on the horizontal (yaw) plane are described. To study the planar motion, we define an inertial reference frame $\{I\}$ and a body-fixed frame $\{B\}$, Fig. 1. The origin of the $\{B\}$ frame coincides with the AUV center of mass (CM) while its axes are along the principal axes of inertia of the vehicle assuming three planes of symmetry: x_b is the longitudinal axis, y_b is the transverse axis, and z_b is the normal axis. Hence, the kinematic equations of motion for an AUV on the horizontal X–Y plane can be written as

$$\begin{bmatrix} \dot{x} \\ \dot{y} \\ \dot{\psi} \end{bmatrix} = \begin{bmatrix} \cos\psi & -\sin\psi & 0 \\ \sin\psi & \cos\psi & 0 \\ 0 & 0 & 1 \end{bmatrix} \begin{bmatrix} u \\ \upsilon \\ r \end{bmatrix}, \quad (1)$$

where x and y represent the inertial coordinates of the CM of the vehicle and u and v are the (linear) surge (forward) and sway (side) velocities, respectively, defined in the body-fixed frame. The orientation of the vehicle is described by the angle ψ measured from the inertial-X axis and r is its yaw (angular) velocity. Assuming that (i) the CM coincides with the center of buoyancy (CB), (ii) the mass distribution is homogeneous, (iii) the hydrodynamic drag terms of order higher than two are negligible, and (iv) the heave, pitch, and roll motions can be neglected, the dynamics for a neutrally buoyant AUV with three planes of symmetry is expressed by the following differential equations:

$$\dot{u} = \frac{m_{22}}{m_{11}} v r - \frac{X_u}{m_{11}} u - \frac{X_{u|u|}}{m_{11}} u|u| + \frac{1}{m_{11}} F_u, \tag{2a}$$

$$\dot{v} = -\frac{m_{11}}{m_{22}} u r - \frac{Y_v}{m_{22}} v - \frac{Y_{v|v|}}{m_{22}} v|v|, \tag{2b}$$

$$\dot{r} = \frac{m_{11} - m_{22}}{m_{33}} u v - \frac{N_r}{m_{33}} r - \frac{N_{r|r|}}{m_{33}} r|r| + \frac{1}{m_{33}} F_r. \tag{2c}$$

The variable F_u denotes the control force along the surge motion of the vehicle and F_r the control torque that is applied in order to produce angular motion around the z_b axis of the body-fixed frame. There is no side thruster to control sway motion; therefore, Eq. (2b) is uncontrolled and the AUV is an underactuated dynamical system. The above control configuration can be realized, e.g., by providing the vehicle with two stern propellers, see Fig. 1. The constants m_{11} and m_{22} are the combined rigid-body and added mass terms, and m_{33} is the combined rigid-body and added moment of inertia about the z_b axis. X_u, $X_{u|u|}$, Y_v, $Y_{v|v|}$, N_r, and $N_{r|r|}$ are the linear and quadratic drag terms coefficients.

3. Trajectory planning

This section describes the trajectory planning methodology. The only restriction on this trajectory is that it must be sufficiently "smooth", i.e., it must be a continuous, inertial, planar curve, and three times differentiable with respect to time.

3.1. Path kinematics

Let us assume that for the tracking control problem, the planar path to be tracked by the CM of an AUV is given as a time function of the inertial variables $x_R(t)$, $y_R(t)$. The subscript "R" indicates a reference variable. The first, second, and third derivatives with respect to time are denoted by $\dot{x}_R(t)$, $\dot{y}_R(t)$, $\ddot{x}_R(t)$, $\ddot{y}_R(t)$, $\dddot{x}_R(t)$, $\dddot{y}_R(t)$. In the remainder of the paper, time dependence notation is omitted.

The magnitude of the velocity vector $\mathbf{v}_P$ of a reference path point P at time t is given by

$$v_p = \|\mathbf{v}_P\| = \|[\dot{x}_R, \dot{y}_R]^T\| = \sqrt{\dot{x}_R^2 + \dot{y}_R^2}. \tag{3}$$

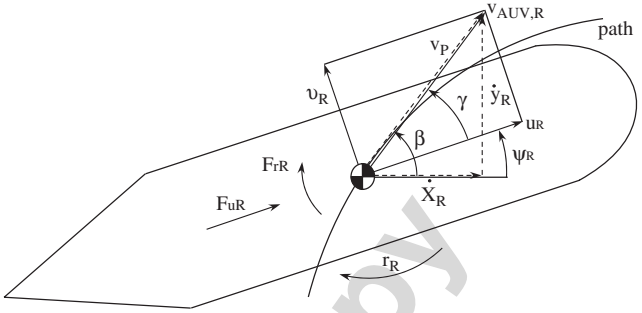

Fig. 2. The AUV moving on a planar path.

The direction of vector $\mathbf{v}_P$ is described by the angle β, see Fig. 2:

$$\beta = \tan^{-1}\left(\frac{\dot{y}_R}{\dot{x}_R}\right). \tag{4}$$

The first and second derivatives of this angle are given by

$$\omega = \dot{\beta} = \frac{\dot{x}_R \ddot{y}_R - \dot{y}_R \ddot{x}_R}{\dot{x}_R^2 + \dot{y}_R^2} \tag{5}$$

$$\Rightarrow \dot{\omega} = f_\omega(\dot{x}_R, \ddot{x}_R, \dddot{x}_R, \dot{y}_R, \ddot{y}_R, \dddot{y}_R), \tag{6}$$

where f_ω indicates that $\dot{\omega}$ is a function of the derivatives of the inertial variables up to the third order. Also, the first and second derivatives of the velocity v_P are

$$\dot{v}_P = \frac{\dot{x}_R \ddot{x}_R + \dot{y}_R \ddot{y}_R}{\sqrt{\dot{x}_R^2 + \dot{y}_R^2}} \tag{7}$$

$$\Rightarrow \ddot{v}_P = f_v(\dot{x}_R, \ddot{x}_R, \dddot{x}_R, \dot{y}_R, \ddot{y}_R, \dddot{y}_R), \tag{8}$$

where f_v indicates that $\ddot{v}_P$ is a function of the derivatives of x_R and y_R.

3.2. AUVs dynamics on the path

The procedure for determining the algebraic and differential equations that relates the inertial reference trajectory variables to the body-fixed velocities, accelerations, and orientation is given next. Let the total linear velocity vector of the AUV be $\mathbf{v}_{AUV} = [u, v]^T$ expressed in the $\{B\}$ frame. Considering the kinematics of the AUV as this tracks the reference trajectory, let u_R, v_R, r_R denote the body-fixed reference velocities. Then, the magnitude of the velocity vector of the CM in $\{B\}$ frame is

$$v_{AUV,R} = \|\mathbf{v}_{AUV,R}\| = \|[u_R, v_R]^T\| = \sqrt{u_R^2 + v_R^2}. \tag{9}$$

As far as the reference orientation ψ_R—the angle between the inertial-X axis and the body-x_b axis, see Fig. 2—is concerned, the following is observed: when the vehicle tracks a generic planar path (with nonzero curvature), the vector $\mathbf{v}_{AUV,R}$ must be tangent to the path. As a result, ψ_R does not coincide with angle β between $\mathbf{v}_{AUV,R}$ and the inertial-X axis but it differs by some angle γ. The latter is created as a consequence of the dynamics of the vehicle as

this rotates. Specifically, looking at Eq. (2b) and considering that the CM of the vehicle tracks the path, we see that because of surge and yaw motions, the coupling term $-(m_{11}/m_{22})u_R r_R$ gives rise to a sway motion v_R. A direct result is the appearance of an angle γ which is expressed as

$$\gamma = \tan^{-1}\left(\frac{v_R}{u_R}\right). \tag{10}$$

Having the description of the path and the states of the AUV as it tracks the path, we conclude that the following geometric conditions must hold: firstly, the magnitude of the tangent vector to the reference path $\mathbf{v}_P$ must equal the magnitude of the vehicle's velocity vector $\mathbf{v}_{AUV,R}$. From Eqs. (3) and (9) it is

$$v_P = v_{AUV,R} \Rightarrow \sqrt{\dot{x}_R^2 + \dot{y}_R^2} = \sqrt{u_R^2 + v_R^2}. \tag{11}$$

Secondly, observing Fig. 2 and considering Eqs. (4) and (10), the relation between the various angles is

$$\psi_R = \beta - \gamma$$
$$\Rightarrow \psi_R = \tan^{-1}\left(\frac{\dot{y}_R}{\dot{x}_R}\right) - \tan^{-1}\left(\frac{v_R}{u_R}\right). \tag{12}$$

Without loss of generality we can assume that the vehicle moves forward, i.e., $u_R > 0$. Then, the sign of γ in Eq. (12) depends on the sign of v_R, which in turn depends on the curvature of the trajectory, i.e., a negative value corresponds to a counterclockwise (CCW) rotation and a positive value to a clockwise (CW) one. From Eq. (11), the reference sway velocity is

$$v_R = \pm\sqrt{\dot{x}_R^2 + \dot{y}_R^2 - u_R^2} = \pm\sqrt{v_P^2 - u_R^2}, \tag{13}$$

where "$\pm$"indicates that v_R may be positive or negative depending on path curvature. For example, if $u_R > 0$ and, $r_R > 0$ then $v_R < 0$. Differentiating Eq. (13) yields

$$\dot{v}_R = \pm\frac{v_P\dot{v}_P - u_R\dot{u}_R}{\sqrt{v_P^2 - u_R^2}}. \tag{14}$$

Also, from Eq. (13) it must be

$$-v_P \leqslant u_R \leqslant v_P, \tag{15}$$

where the equality holds in the case of straight line tracking or when a change in the sign of the curvature occurs (then $v_R = r_R = 0$). The reference angular velocity and acceleration that correspond to the path are obtained by differentiating twice ψ_R in Eq. (12) and taking into account Eqs. (5), (7) and (13), to yield,

$$r_R = \dot{\psi}_R = \frac{d}{dt}\left[\tan^{-1}\left(\frac{\dot{y}_R}{\dot{x}_R}\right) - \tan^{-1}\left(\frac{\sqrt{v_P^2 - u_R^2}}{u_R}\right)\right]$$
$$= \omega - \frac{u_R\dot{v}_P - \dot{u}_R v_P}{v_P\sqrt{v_P^2 - u_R^2}} \tag{16}$$

$$\Rightarrow \dot{r}_R = f_r(\omega, \dot{\omega}, u_R, \dot{u}_R, \ddot{u}_R, v_P, \dot{v}_P, \ddot{v}_P). \tag{17}$$

What remains now is the computation of the surge u_R—assumed positive—velocity. For a CW rotation (CW-type path), using the fact that $v_R > 0$, and substituting the appropriate expressions in Eqs. (14), (13), and (16) that give $\dot{v}_R, v_R$, and r_R in (2b), the following differential equation results whose solution yields the reference surge velocity:

$$\dot{u}_R = [(m_{11} - m_{22})u_R v_P^3]^{-1}\{-v_P^3(m_{22}v_P\dot{v}_P + Y_v(v_P^2 - u_R^2))$$
$$+ m_{11}u_R[u_R\dot{v}_P v_P^2 + v_P\sqrt{v_P^2 - u_R^2}(\ddot{x}_R\dot{y}_R - \dot{x}_R\ddot{y}_R)]$$
$$- Y_{v|v|}(v_P^2 - u_R^2)v_P^3|\sqrt{v_P^2 - u_R^2}|\}. \tag{18}$$

For a CCW rotation (CCW-type path), it is $v_R < 0$ and $r_R > 0$, yielding,

$$\dot{u}_R = [(m_{11} - m_{22})u_R v_P^3]^{-1}\{-v_P^3(m_{22}v_P\dot{v}_P + Y_v(v_P^2 - u_R^2))$$
$$+ m_{11}u_R[u_R\dot{v}_P v_P^2 + v_P\sqrt{v_P^2 - u_R^2}(\dot{x}_R\ddot{y}_R - \ddot{x}_R\dot{y}_R)]$$
$$- Y_{v|v|}(v_P^2 - u_R^2)v_P^3|\sqrt{v_P^2 - u_R^2}|\}. \tag{19}$$

For a general motion in which the curvature of the path changes with time, we switch between the above differential equations. The initial condition $u_{R,o} = u_R\ (t = 0)$ is used with the appropriate differential equation. As the integration progresses and switches between the two equations, the initial condition for the current equation is the last value obtained from the integration of the previous equation. Numerical integration of the appropriate equation between Eqs. (18) and (19) yields $u_R(t)$. Using the computed u_R along with v_R, $\dot{x}_R$, $\dot{y}_R$, and Eq. (12), we compute the AUV reference orientation, $\psi_R(t)$.

Thus far, the feasible trajectory including the feasible orientation is completely known. Also, all the feasible body-fixed velocities and accelerations, required for tracking, have been computed. Using the AUV dynamic model, it is straightforward now to compute the corresponding open-loop control efforts. Indeed, from Eqs. (2a) and (2c), these controls are given by

$$F_{uR} = m_{11}\dot{u}_R - m_{22}v_R r_R + X_u u_R + X_{u|u|}u_R^2, \tag{20}$$

$$F_{rR} = m_{33}\dot{r}_R + (m_{22} - m_{11})u_R v_R + N_r r_R - N_{r|r|}r_R^2. \tag{21}$$

The presented trajectory planning algorithm and the open-loop control efforts given by Eqs. (20) and (21) can be incorporated in a two-step closed-loop trajectory-tracking controller design. Forward feeding the actuators of an AUV with the above open-loop controls, consistent with the vehicle dynamics, allows one to design a feedback controller for taking care of the small tracking errors due to model parameter uncertainty, external disturbances, etc. It is expected that such a controller will not require large gains and, hence, will exhibit an improved performance. In Section 4, we exploit the benefits mentioned above by designing such a closed-loop controller.

In the next two subsections, we give examples of planar paths, each of which presents special characteristics. The first is a circular path in which, although the reference body-fixed velocities are constant, the body-x_b axis of the AUV must rotate sufficiently towards the inside of the

Table 1
Rigid body and hydrodynamic parameters of the AUV studied by Pettersen and Egeland (1999)

Parameter	Symbol	Value	Unit
Mass	m	185	kg
Rotational inertia	I_z	50	kg m^2
Added mass	$X_{\dot{u}}$	−30	kg
Added mass	$Y_{\dot{v}}$	−80	kg
Added mass	$N_{\dot{r}}$	−30	kg m^2
Surge linear drag	X_u	70	kg/s
Surge quadratic drag	$X_{u\|u\|}$	100	kg/m
Sway linear drag	Y_v	100	kg/s
Sway quadratic drag	$Y_{v\|v\|}$	200	kg/m
Yaw linear drag	N_r	50	kg m^2/s
Quadratic yaw drag	$N_{r\|r\|}$	100	kg m^2

circle—by an angle γ—in order to counteract the constant centrifugal force. The second is a sinusoidal path in which all of the body-fixed velocities are time-varying. In this case, the relative orientation of the body-x_b axis with respect to the tangent vector to the curve—$\mathbf{v}_P$—also changes with time. The various system parameters for a typical AUV, used for simulation purposes, are given in Table 1.

Also,

$$m_{11} = m - X_{\dot{u}} = 215 \text{ kg},$$
$$m_{22} = m - Y_{\dot{v}} = 265 \text{ kg},$$
$$m_{33} = I_z - N_{\dot{r}} = 80 \text{ kg m}^2, \quad (22)$$

where the constants m_{ii} $(i = 1, \ldots, 3)$ are constants representing the combined inertia and added mass terms.

3.3. Reference paths

3.3.1. Circular path

We consider a reference circular inertial planar trajectory, described as follows:

$$x_R(t) = 10 \sin(0.01t) \text{ m}, \quad (23a)$$

$$y_R(t) = 10 \cos(0.01t) \text{ m}. \quad (23b)$$

Here, the derivatives up to the *second order* are needed, since tracking the above circle is obtained by the vehicle with constant linear velocities u_R and v_R and angular velocity r_R. Using Eqs. (3) and (7), we find that $v_P = 0.1$ m/s and $\dot{v}_P = 0$. Also from Eq. (5), $\omega = -0.01$ rad/s, meaning a constant CW-type path. Forward tracking of this circle requires the reference body-fixed velocities of the AUV signed as $u_R > 0$, $v_R > 0$, and $r_R < 0$. Their values are computed as follows: in Eq. (18), we substitute v_P, and $\dot{x}_R(t)$, $\dot{y}_R(t)$, $\ddot{x}_R(t)$, $\ddot{y}_R(t)$, for their previously computed values. We also substitute the constant terms for their numerical values from Table 1. Solving numerically the differential equation that corresponds to the CW sense of the circle with $u_R(0) = 10^{-3}$, we obtain $u_R = 0.099$ m/s and $\dot{u}_R = 0$. Using Eqs. (13), (14), and (16) with the appropriate substitutions it is easy now to obtain $v_R = 0.0021$ m/s, $\dot{v}_R = 0$, $r_R = -0.01$ rad/s, and $\dot{r}_R = 0$. Additionally, from Eq. (10) it is found that $\gamma = 1.23°$, which means that during tracking the body-x_b axis must point towards the inside of the circle. From Eqs. (20) and (21), the constant open-loop control force and torque are computed as $F_{uR} = 8.003$ N and $F_{rR} = -0.5$ Nm.

3.3.2. Sinusoidal path

The required velocities for the tracking of the previous circular trajectory were constant. Here, we show that the methodology developed in this section is applicable in the case where the velocities vary with time, i.e., the accelerations must be taken into account. This methodology, combined with the closed-loop controller that will be designed later, offers to the guidance and control design task greater flexibility since it provides the capability of tracking *any smooth path* with time-varying velocities, as opposed to the usual "trimming" trajectories, i.e., trajectories with constant velocities. Note that the derivatives of the inertial position variables up to the *third order* are needed. As an illustration, we selected a planar path which itself is of practical interest for the operation of an AUV: the sinusoidal curve. For example, such a path may allow an AUV to sweep an orthogonal area of the sea bottom. The equations that describe the curve are

$$x_R(t) = 0.03t \text{ m}, \quad (24a)$$

$$y_R(t) = 10 \sin(0.03t) \text{ m}. \quad (24b)$$

The presentation of the methodology in the case of the sinusoidal path is best assisted using Fig. 3.

In Fig. 3(a), we observe the following: the vector $\mathbf{v}_P$ is always tangent to the curve. The velocity u_R always points inside the curve and, in this example, it is always positive meaning forward motion; its magnitude changes from a maximum value $u_{R,max} = 0.3$ m/s—equal to v_P—at zero curvature point B, to a minimum value $u_{R,min} = 0.02$ m/s at maximum curvature points, i.e., at curve peaks (b) and (e). In order to describe the behavior of the reference sway velocity v_R and the reference yaw velocity r_R (not sketched in the figure for clarity), we distinguish two sections in the above curve: section AB in which the required rotation is CCW and, hence, according to what we have considered so far, it is $v_R < 0$ and $r_R > 0$, and section BC where the required rotation is CW with $v_R > 0$ and $r_R < 0$. They both take their absolute maximum values at the points with the maximum curvature, i.e., at the curve peaks, where $|v_{R,max}| = |v_{R,min}| = 0.018$ m/s and $|r_{R,max}| = |r_{R,min}| = 0.326$ rad/s. At the point where these two sections meet, i.e., the zero curvature point B, $v_R = r_R = 0$. Considering now the time-evolution of the various angles we have the following: the values of the angles ψ_R and β are measured with respect to the inertial-X axis; they are positive in the CCW sense. Tracking the sinusoidal path results in altering

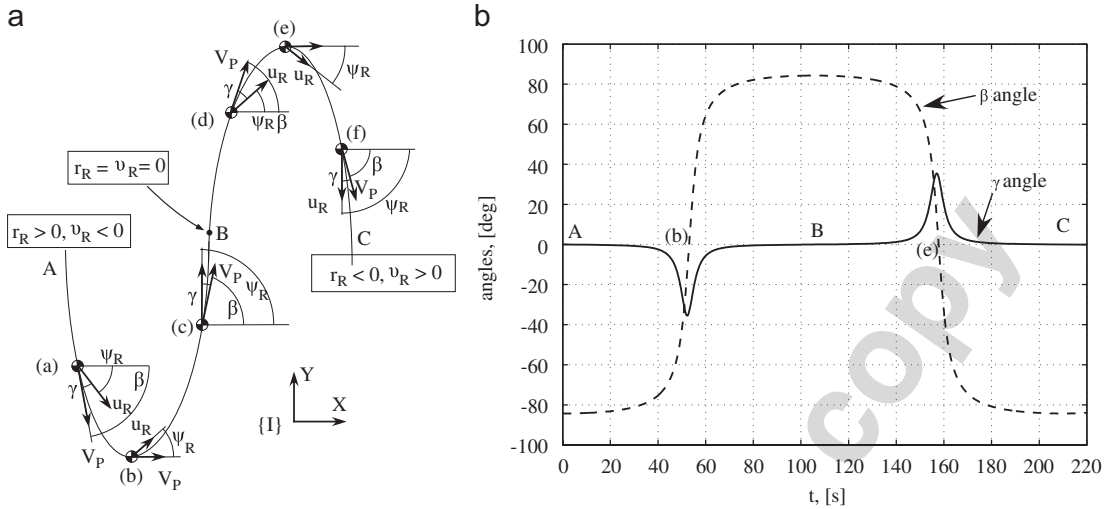

Fig. 3. (a) The sinusoidal path with the reference velocities, orientation and the angles β and γ. (b) Time evolution of the angles β and γ for one period of the sinusoidal function.

their sign and their relative position as one can see in Fig. 3. As far as the angle γ concerns, taking into consideration its definition from Eq. (10), we see that its sign follows that of υ_R—since $u_R > 0$—and its magnitude varies analogously, see Fig. 3(b). The calculation of the body-fixed velocities, accelerations, and orientation and, finally, the required open-loop controls results from the utilization of Eqs. (3)–(21).

From the preceding trajectory planning methodology we conclude the following: the reference orientation ψ_R of the vehicle does not coincide with the angle between the velocity vector $\mathbf{v}_P$ and the inertial-X axis but it depends on trajectory characteristics such as time-parameterization, differentiability, etc., and, of course, on vehicle dynamics. Actuator saturation limits also play a crucial role in the kind of trajectories that can be tracked.

The above analysis holds when the AUV is "on the path" i.e., position, orientation, and velocity errors are zero for time $t \geqslant 0$. In cases such as when the vehicle deviates from the trajectory, or when there are modeling errors or external disturbances, the open-loop control does not suffice; a closed-loop trajectory-tracking controller is needed to guide the vehicle to the reference trajectory, drive the corresponding errors as close as possible to zero and keep the vehicle on the path even in the case of external disturbances, e.g., sea currents. This is discussed next.

4. Closed-loop tracking control

4.1. Error dynamics formulation

Using the states of the AUV—inertial position and orientation, and body-fixed velocities—and the corresponding reference variables previously computed, the tracking errors are defined as

$$\begin{aligned} u_e &= u - u_R, \\ \upsilon_e &= \upsilon - \upsilon_R, \\ r_e &= r - r_R, \\ x_e &= x - x_R, \\ y_e &= y - y_R, \\ \psi_e &= \psi - \psi_R. \end{aligned} \tag{25}$$

Substituting for $u, \upsilon, r, x, y, \psi$, in Eqs. (1) and (2) we obtain the error dynamics as follows. Firstly, using Eqs. (1) and (25) the error kinematics can be written as

$$\begin{bmatrix} \dot{x}_e \\ \dot{y}_e \end{bmatrix} = \begin{bmatrix} \cos\psi & -\sin\psi \\ \sin\psi & \cos\psi \end{bmatrix} \begin{bmatrix} u_e \\ \upsilon_e \end{bmatrix} + \begin{bmatrix} \cos\psi - \cos\psi_R & -\sin\psi + \sin\psi_R \\ \sin\psi - \sin\psi_R & \cos\psi - \cos\psi_R \end{bmatrix} \begin{bmatrix} u_R \\ \upsilon_R \end{bmatrix}$$

$$\Rightarrow \dot{\mathbf{x}}_e = \mathbf{R}\mathbf{u}_e + \mathbf{R}_{\psi,\psi_R}\mathbf{u}_R \tag{26a}$$

$$\Rightarrow \dot{\mathbf{x}}_e = \mathbf{R}\mathbf{u}_e + \boldsymbol{\delta}, \tag{26b}$$

$$\dot{\psi}_e = r_e, \tag{26c}$$

where

$$\dot{\mathbf{x}}_e \triangleq [\dot{x}_e, \dot{y}_e]^T,$$

$$\mathbf{u}_e \triangleq [u_e, \upsilon_e]^T,$$

$$\mathbf{R} \triangleq \mathbf{R}(\psi) = \begin{bmatrix} \cos\psi & -\sin\psi \\ \sin\psi & \cos\psi \end{bmatrix},$$

$$\mathbf{R}_{\psi,\psi_R} \triangleq \mathbf{R}(\psi) - \mathbf{R}(\psi_R),$$

$$\mathbf{u}_R \triangleq [u_R, \upsilon_R]^T,$$

$\boldsymbol{\delta} \triangleq \mathbf{R}_{\psi,\psi_R}\mathbf{u}_R$.

Using Eqs. (2) and (25) the error dynamics is derived as,

$$\begin{aligned}\dot{u}_e = {} & \frac{m_{22}}{m_{11}}(v_e r_e + v_e r_R + v_R r_e) - \frac{X_u}{m_{11}}u_e - \dot{u}_R \\ & + \frac{m_{22}}{m_{11}}v_R r_R - \frac{X_u}{m_{11}}u_R - \frac{X_{u|u|}}{m_{11}} \\ & \times(u_e + u_R)|u_e + u_R| + \frac{F_u}{m_{11}}\end{aligned} \tag{27a}$$

$$\begin{aligned}\dot{v}_e = {} & -\frac{m_{11}}{m_{22}}(u_e r_e + u_e r_R + u_R r_e) - \frac{Y_v}{m_{22}}v_e - \dot{v}_R \\ & - \frac{m_{11}}{m_{22}}u_R r_R - \frac{Y_v}{m_{22}}v_R - \frac{Y_{v|v|}}{m_{22}} \\ & \times(v_e + v_R)|v_e + v_R|,\end{aligned} \tag{27b}$$

$$\begin{aligned}\dot{r}_e = {} & \frac{m_{11} - m_{22}}{m_{33}}(u_e v_e + u_e v_R + u_R v_e) - \frac{N_r}{m_{33}}r_e - \dot{r}_R \\ & + \frac{m_{11} - m_{22}}{m_{33}}u_R v_R - \frac{N_r}{m_{33}}r_R \\ & - \frac{N_{r|r|}}{m_{33}}(r_e + r_R)|r_e + r_R| + \frac{F_r}{m_{33}}\end{aligned} \tag{27c}$$

In the above equations, when the error variables are zero, we observe that the remaining dynamical system reduces to the reference one with $F_u = F_{uR}$ and $F_r = F_{rR}$, as computed in Section 3.

4.2. Error dynamics stabilization

Having completed the derivation of the error dynamics, the control objective is to stabilize them. In this way, the tracking control problem is transformed to an easier to handle stabilization one. The nonerror variables, i.e., the reference ones, are treated as time varying parameters making the system a time-varying (non-autonomous) system. Setting,

$$\begin{aligned}F_u = {} & -m_{22}(v_e r_e + v_e r_R + v_R r_e) + X_u u_e + m_{11}\dot{u}_R \\ & - m_{22}v_R r_R + X_u u_R + X_{u|u|} \\ & \times(u_e + u_R)|u_e + u_R| + m_{11}\tau_u\end{aligned} \tag{28a}$$

$$\begin{aligned}F_r = {} & (m_{22} - m_{11})(u_e v_e + u_e v_R + u_R v_e) + N_r r_e + m_{33}\dot{r}_R \\ & - (m_{11} - m_{22})u_R v_R + N_r r_R + N_{r|r|} \\ & \times(r_e + r_R)|r_e + r_R| + m_{33}\tau_r\end{aligned} \tag{28b}$$

yields a partial linearized system, described by

$$\dot{u}_e = \tau_u \tag{29a}$$

$$\begin{aligned}\dot{v}_e = {} & -\frac{m_{11}}{m_{22}}(u_e r_e + u_e r_R + u_R r_e) - \frac{Y_v}{m_{22}}v_e - \dot{v}_R \\ & - \frac{m_{11}}{m_{22}}u_R r_R - \frac{Y_v}{m_{22}}v_R - \frac{Y_{v|v|}}{m_{22}}(v_e + v_R)|v_e + v_R|,\end{aligned} \tag{29b}$$

$$\dot{r}_e = \tau_r, \tag{29c}$$

$$\begin{aligned}\begin{bmatrix}\dot{x}_e \\ \dot{y}_e\end{bmatrix} = {} & \begin{bmatrix}\cos\psi & -\sin\psi \\ \sin\psi & \cos\psi\end{bmatrix}\begin{bmatrix}u_e \\ v_e\end{bmatrix} \\ & + \begin{bmatrix}\cos\psi - \cos\psi_R & -\sin\psi + \sin\psi_R \\ \sin\psi - \sin\psi_R & \cos\psi - \cos\psi_R\end{bmatrix} \\ & \times\begin{bmatrix}u_R \\ v_R\end{bmatrix},\end{aligned} \tag{29d, e}$$

$$\dot{\psi}_e = r_e. \tag{29f}$$

Here, τ_u and τ_r are auxiliary control design variables.

Examination of Eqs. (29) shows that there is direct control capability on the forward (surge) and on the rotational motion of the vehicle but not on the side (sway) motion, i.e., we can control the linear velocity u and the corresponding error u_e as well as the angular velocity r and the corresponding error r_e. We also observe that we have indirect control of the side velocity error v_e through the coupling of the controlled variables in the term $-m_{11}/m_{22}\,(u_e r_e + u_e r_R + u_R r_e)$. Consistent with backstepping design techniques, for the side velocity error v_e, we can choose as an auxiliary control variable one of the controlled velocities and, then, stabilize the latter using the corresponding actual control variable. The same observations hold for the linear and angular position errors: we first use the velocities as control variables for the position and, in a following step, we stabilize the velocities u_e and r_e with τ_u and τ_r and v_e using the aforementioned coupling term. Next, backstepping and nonlinear damping are employed as our design tools (Krstic et al., 1995).

Step 1: Considering the subsystem of Eqs. (29d)–(29f), we take as auxiliary control the vector $\mathbf{u}_e = [u_e, v_e]^T$ and as a bounded disturbance (for bounded u_R and v_R) the vector $\boldsymbol{\delta} = [\delta_1, \delta_2]^T$. Choosing

$$V_1 = \tfrac{1}{2}\mathbf{x}_e^T\mathbf{x}_e. \tag{30}$$

The desired expressions for the virtual controls are

$$\mathbf{u}_{e,des} = -\mathbf{R}^T[\mathbf{K} + \mathbf{K}_1]\mathbf{x}_e \triangleq \boldsymbol{\alpha}(\mathbf{x}_e) = [\alpha_u, \alpha_v]^T, \tag{31}$$

where

$$\boldsymbol{\alpha}(\mathbf{x}_e) = \begin{bmatrix}\alpha_u \\ \alpha_v\end{bmatrix} = \begin{bmatrix}-(k + k_1)x_e\cos\psi - (k + k_1)y_e\sin\psi \\ (k + k_1)x_e\sin\psi - (k + k_1)y_e\cos\psi\end{bmatrix}, \tag{32}$$

$$\mathbf{K} = \mathrm{diag}(k, k), \quad \mathbf{K}_1 = \mathrm{diag}(k_1, k_1). \tag{33}$$

with $\mathbf{K}$ and $\mathbf{K}_1$ are positive definite matrices. Then, the time derivative of V_1 in Eq. (30) becomes

$$\dot{V}_1 = -\mathbf{x}_e^T(\mathbf{K} + \mathbf{K}_1)\mathbf{x}_e + \mathbf{x}_e^T\boldsymbol{\delta}. \tag{34}$$

The quantity $\boldsymbol{\delta}$ is a bounded function of the desired linear velocities; considering the worst case for the sign of the quantity $\mathbf{x}_e^T\boldsymbol{\delta}$, i.e., positive, we conclude that when the vehicle moves fast, there may be paths that the vehicle cannot track accurately. In order to further reduce the effects of this quantity on the negativity of the derivative of

V_1, we use the gain matrix $\mathbf{K}_1$ as follows:

$$\begin{aligned}\dot{V}_1 =& -\mathbf{x}_e^T\mathbf{K}\mathbf{x}_e - \mathbf{x}_e^T\mathbf{K}_1\mathbf{x}_e + \mathbf{x}_e^T\boldsymbol{\delta}\\ =& -\mathbf{x}_e^T\mathbf{K}\mathbf{x}_e - k_1\left(x_e - \frac{\delta_1}{2k_1}\right)^2\\ & - k_1\left(y_e - \frac{\delta_2}{2k_1}\right)^2 + \frac{\|\boldsymbol{\delta}\|^2}{4k_1}.\end{aligned} \tag{35}$$

Increasing the gain k_1 diminishes the quantity $\|\boldsymbol{\delta}\|^2/4k_1$.

Step 2: The components of the vector $[u_e, v_e]^T$ are not true controls, thus we have to introduce appropriate error variables z_u and z_v defined as

$$\mathbf{z}_u = [z_u, z_v]^T = [u_e - \alpha_u, v_e - \alpha_v]^T. \tag{36}$$

Then, the controlled position equations are rewritten as

$$\dot{\mathbf{x}}_e = -\mathbf{K}\mathbf{x}_e - \mathbf{K}_1\mathbf{x}_e + \mathbf{R}\mathbf{z}_u + \boldsymbol{\delta}. \tag{37}$$

We compute now the following derivatives:

$$\dot{\alpha}_u = -(k+k_1)u_e - (k+k_1)(\delta_1\cos\psi + \delta_2\sin\psi), \tag{38a}$$

$$\dot{\alpha}_v = -(k+k_1)v_e + (k+k_1)(\delta_1\sin\psi + \delta_2\cos\psi). \tag{38b}$$

Then, the linear velocities equations, using the new variables, are rewritten as

$$\dot{z}_u = \tau_u + (k+k_1)u_e + (k+k_1)(\delta_1\cos\psi + \delta_2\sin\psi), \tag{39a}$$

$$\begin{aligned}\dot{z}_v =& -\frac{m_{11}}{m_{22}}(u_e r_e + u_e r_R + u_R r_e) - \frac{Y_v}{m_{22}}v_e - \dot{v}_R - \frac{m_{11}}{m_{22}}u_R r_R\\ & - \frac{Y_v}{m_{22}}v_R - \frac{Y_{v|v|}}{m_{22}}(v_e + v_R)|v_e + v_R|\\ & + [(k+k_1)v_e - (k+k_1)(\delta_1\sin\psi - \delta_2\cos\psi)].\end{aligned} \tag{39b}$$

The task now is to stabilize the error vector $\mathbf{z}_u$. In this step, we design control to stabilize the component z_u. Choosing

$$V_2 = V_1 + \tfrac{1}{2}z_u^2 \tag{40}$$

its time derivative becomes

$$\begin{aligned}\dot{V}_2 =& \dot{V}_1 + z_u\dot{z}_u\\ & \Rightarrow \dot{V}_2 = \mathbf{x}_e^T[-(\mathbf{K}+\mathbf{K}_1)\mathbf{x}_e + \mathbf{R}\mathbf{z}_u + \boldsymbol{\delta}]\\ & + z_u[\tau_u + (k+k_1)u_e\\ & + (k+k_1)(\delta_1\cos\psi + \delta_2\sin\psi)].\end{aligned} \tag{41}$$

Taking into account Eq. (35) and after straightforward algebraic manipulations, Eq. (41) yields

$$\begin{aligned}\dot{V}_2 =& -\mathbf{x}_e^T\mathbf{K}\mathbf{x}_e - k_1\left(x_e - \frac{\delta_1}{2k_1}\right)^2 - k_1\left(y_e - \frac{\delta_2}{2k_1}\right)^2 + \frac{\|\boldsymbol{\delta}\|^2}{4k_1}\\ & + z_u[\tau_u + x_e\cos\psi + y_e\sin\psi + (k+k_1)u_e\\ & + (k+k_1)(\delta_1\cos\psi + \delta_2\sin\psi)]\\ & + z_v(y_e\cos\psi - x_e\sin\psi).\end{aligned}$$

Setting

$$\begin{aligned}\tau_u =& -c_u z_u - c_{3u}z_u^3 - (x_e\cos\psi + y_e\sin\psi) - (k+k_1)u_e\\ & - (k+k_1)(\delta_1\cos\psi + \delta_2\sin\psi) + f_u,\end{aligned} \tag{42}$$

where f_u is a design variable for subsequent use, the previous derivative becomes

$$\begin{aligned}\dot{V}_2 =& -\mathbf{x}_e^T\mathbf{K}\mathbf{x}_e - k_1\left(x_e - \frac{\delta_1}{2k_1}\right)^2 - k_1\left(y_e - \frac{\delta_2}{2k_1}\right)^2 + \frac{\|\boldsymbol{\delta}\|^2}{4k_1}\\ & - c_u z_u^2 - c_{3u}z_u^4 + z_u f_u + z_v(y_e\cos\psi - x_e\sin\psi).\end{aligned} \tag{43}$$

So far, the controlled subsystem of error dynamics equations has been transformed to

$$\begin{aligned}\dot{\mathbf{x}}_e =& -\mathbf{K}\mathbf{x}_e - \mathbf{K}_1\mathbf{x}_e + \mathbf{R}\mathbf{z}_u + \boldsymbol{\delta}\\ \dot{z}_u =& -c_u z_u - c_{3u}z_u^3 - (x_e\cos\psi + y_e\sin\psi) + f_u.\end{aligned} \tag{44}$$

Before proceeding to the next step of the design, we perform some manipulations on the sway error dynamics equation yielding

$$\begin{aligned}\dot{z}_v =& -\frac{m_{11}}{m_{22}}ur_e - \frac{m_{11}}{m_{22}}r_R z_u + \frac{m_{11}}{m_{22}}r_R(k+k_1)\\ & \times(x_e\cos\psi + y_e\sin\psi) + \left[(k+k_1) - \frac{Y_v}{m_{22}}\right]v_e\\ & - \dot{v}_R - \frac{m_{11}}{m_{22}}u_R r_R - \frac{Y_v}{m_{22}}v_R - \frac{Y_{v|v|}}{m_{22}}v|v|\\ & - (k+k_1)(v_R\cos\psi_e - u_R\sin\psi_e - v_R).\end{aligned} \tag{45}$$

In the above equation we set

$$\begin{aligned}\delta_v =& \frac{m_{11}}{m_{22}}r_R(k+k_1)(x_e\cos\psi + y_e\sin\psi)\\ & + \left[(k+k_1) - \frac{Y_v}{m_{22}}\right]v_e - \dot{v}_R - \frac{m_{11}}{m_{22}}u_R r_R - \frac{Y_v}{m_{22}}v_R\\ & - \frac{Y_{v|v|}}{m_{22}}v|v| - (k+k_1)(v_R\cos\psi_e - u_R\sin\psi_e - v_R).\end{aligned} \tag{46}$$

Temporarily, we will treat this as a time-varying variable and deal with it later, at the final step. We rewrite Eq. (45) as

$$\dot{z}_v = -\frac{m_{11}}{m_{22}}ur_e - \frac{m_{11}}{m_{22}}r_R z_u + \delta_v. \tag{47}$$

Step 3: The next subsystem to stabilize consists of Eqs. (29f) and (47). Considering the error $r_e = \alpha_r$ as an auxiliary control, assuming $u \neq 0$ a natural requirement for tracking, choosing

$$V_3 = V_2 + (z_v^2 + \psi_e^2)/2 \tag{48}$$

and taking into account Eq. (43), it is

$$\begin{aligned}\dot{V}_3 =& -\mathbf{x}_e^T\mathbf{K}\mathbf{x}_e - k_1\left(x_e - \frac{\delta_1}{2k_1}\right)^2 - k_1\left(y_e - \frac{\delta_2}{2k_1}\right)^2 + \frac{\|\boldsymbol{\delta}\|^2}{4k_1}\\ & - c_u z_u^2 - c_{3u}z_u^4 + z_u\left(f_u - \frac{m_{11}}{m_{22}}r_R z_v\right)\\ & + z_v(y_e\cos\psi - x_e\sin\psi)\\ & + \left(-\frac{m_{11}}{m_{22}}uz_v + \psi_e\right)\alpha_r + z_v\delta_v.\end{aligned} \tag{49}$$

Setting

$$\alpha_r = -c_r\left(-\frac{m_{11}}{m_{22}}uz_v + \psi_e\right) \tag{50}$$

for some c_r positive we obtain

$$\begin{aligned}\dot{V}_3 = & -\mathbf{x}_e^T\mathbf{K}\mathbf{x}_e - k_1\left(x_e - \frac{\delta_1}{2k_1}\right)^2 \\ & - k_1\left(y_e - \frac{\delta_2}{2k_1}\right)^2 + \frac{\|\boldsymbol{\delta}\|^2}{4k_1} \\ & - c_u z_u^2 - c_{3u} z_u^4 + z_u\left(f_u - \frac{m_{11}}{m_{22}} r_R z_v\right) \\ & + z_v(y_e\cos\psi - x_e\sin\psi) \\ & - c_r\left(-\frac{m_{11}}{m_{22}} u z_v + \psi_e\right)^2 + z_v\delta_v. \end{aligned} \tag{51}$$

Step 4: The variable $r_e = \alpha_r$ is not a true control. Thus, we have to introduce an error $z_r = r_e - \alpha_r$ in place of α_r and we use τ_r to stabilize the subsystem:

$$\dot{z}_v = -\frac{m_{11}}{m_{22}} u r_e - \frac{m_{11}}{m_{22}} r_R z_u + \delta_v, \tag{52a}$$

$$\dot{\psi}_e = \alpha_r + z_r, \tag{52b}$$

$$\dot{z}_r = \tau_r - \dot{\alpha}_r, \tag{52c}$$

where

$$\dot{\alpha}_r = -c_r\left[\left(\frac{m_{11}}{m_{22}} u\right)^2 + 1\right] r_e + c_r\frac{m_{11}}{m_{22}} u\delta_v - c_r\left(\frac{m_{11}}{m_{22}}\right)^2 u r_R z_u. \tag{53}$$

So far, the dynamic equations are

$$\begin{aligned}\dot{\mathbf{x}}_e = & -\mathbf{K}\mathbf{x}_e - \mathbf{K}_1\mathbf{x}_e + \mathbf{R}\mathbf{z}_u + \boldsymbol{\delta}, \\ \dot{z}_u = & -c_u z_u - c_{3u} z_u^3 - (x_e\cos\psi + y_e\sin\psi) + f_u, \\ \dot{z}_v = & -c_r\left(\frac{m_{11}}{m_{22}} u\right)^2 z_v + c_r\left(\frac{m_{11}}{m_{22}} u\right)\psi_e \\ & - \left(\frac{m_{11}}{m_{22}} u\right) z_r - \frac{m_{11}}{m_{22}} r_R z_u + \delta_v, \\ \dot{\psi}_e = & \, c_r\frac{m_{11}}{m_{22}} u z_v - c_r\psi_e + z_r, \\ \dot{z}_r = & \, \tau_r - \dot{\alpha}_r. \end{aligned} \tag{54}$$

Finally, for the complete system, we choose

$$V_4 = V_3 + z_r^2/2 \tag{55}$$

and taking the derivative we obtain

$$\begin{aligned}\dot{V}_4 = & -\mathbf{x}_e^T\mathbf{K}\mathbf{x}_e - k_1\left(x_e - \frac{\delta_1}{2k_1}\right)^2 \\ & - k_1\left(y_e - \frac{\delta_2}{2k_1}\right)^2 + \frac{\|\boldsymbol{\delta}\|^2}{4k_1} - c_u z_u^2 - c_{3u} z_u^4 \\ & + z_u\left(f_u - \frac{m_{11}}{m_{22}} r_R z_v\right) + z_v(y_e\cos\psi - x_e\sin\psi) \\ & - c_r\left(\frac{m_{11}}{m_{22}} u\right)^2 z_v^2 + 2c_r\left(\frac{m_{11}}{m_{22}} u\right)\psi_e z_v \\ & + z_v\delta_v - c_r\psi_e^2 - z_v z_r \\ & + z_r\left[\tau_r + \psi_e + z_v - \left(\frac{m_{11}}{m_{22}} u\right) z_v + c_r\left[\left(\frac{m_{11}}{m_{22}} u\right)^2 + 1\right] r_e\right. \\ & \left. - c_r\frac{m_{11}}{m_{22}} u\delta_v + c_r\left(\frac{m_{11}}{m_{22}}\right)^2 u r_R\right]. \end{aligned} \tag{56}$$

With positive c and c_3, we set

$$\begin{aligned}\tau_r = & -\psi_e - z_v - c z_r - c_3 z_r^3 + \left(\frac{m_{11}}{m_{22}} u\right) z_v \\ & - c_r\left[\left(\frac{m_{11}}{m_{22}} u\right)^2 + 1\right] r_e + c_r\frac{m_{11}}{m_{22}} u\delta_v \\ & - c_r\left(\frac{m_{11}}{m_{22}}\right)^2 u r_R z_u. \end{aligned} \tag{57}$$

Then, derivative becomes

$$\begin{aligned}\dot{V}_4 = & -\mathbf{x}_e^T\mathbf{K}\mathbf{x}_e - k_1\left(x_e - \frac{\delta_1}{2k_1}\right)^2 \\ & - k_1\left(y_e - \frac{\delta_2}{2k_1}\right)^2 + \frac{\|\boldsymbol{\delta}\|^2}{4k_1} \\ & - c_u z_u^2 - c_{3u} z_u^4 + z_u\left(f_u - \frac{m_{11}}{m_{22}} r_R z_v\right) \\ & + z_v(y_e\cos\psi - x_e\sin\psi) \\ & - c_r\left(\frac{m_{11}}{m_{22}} u\right)^2 z_v^2 + 2c_r\left(\frac{m_{11}}{m_{22}} u\right)\psi_e z_v \\ & + z_v\delta_v - c_r\psi_e^2 - z_v z_r - c z_r^2 - c_3 z_r^4. \end{aligned} \tag{58}$$

In order to deal with the quantities with uncertain sign we conduct some algebraic manipulations. Firstly, we set

$$f_u = \frac{m_{11}}{m_{22}} r_R z_v - c_4 z_u z_v^2 - c_5 z_u z_v^4. \tag{59}$$

Then, Eq. (58) becomes

$$\begin{aligned}\dot{V}_4 = & -\mathbf{x}_e^T\mathbf{K}\mathbf{x}_e - k_1\left(x_e - \frac{\delta_1}{2k_1}\right)^2 - k_1\left(y_e - \frac{\delta_2}{2k_1}\right)^2 + \frac{\|\boldsymbol{\delta}\|^2}{4k_1} \\ & - c_u z_u^2 - c_{3u} z_u^4 - c_4 z_u^2 z_v^2 - c_5 z_u^2 z_v^4 \\ & - c_r\left(\frac{m_{11}}{m_{22}} u\right)^2 z_v^2 - c_r\psi_e^2 - c z_r^2 - c_3 z_r^4 \\ & + z_v(y_e\cos\psi - x_e\sin\psi) + 2c_r\left(\frac{m_{11}}{m_{22}} u\right)\psi_e z_v \\ & - z_v z_r + z_v\delta_v. \end{aligned} \tag{60}$$

Now, the last four terms with uncertain sign are examined using a worst case analysis, i.e., considering that all of them are positive. In the following analysis we use Young's inequality; the quantities ε_i, $i = 1, \ldots, 8$, are positive constants. For the first three of the uncertain terms we have

$$\begin{aligned} & z_v(y_e\cos\psi - x_e\sin\psi) \\ & \leqslant \frac{1}{4\varepsilon_1}|y_e|^2 + \varepsilon_1|z_v|^2 + \frac{1}{4\varepsilon_1}|x_e|^2 + \varepsilon_1|z_v|^2, \end{aligned} \tag{61}$$

$$2c_r\left(\frac{m_{11}}{m_{22}}u\right)\psi_e z_v \leqslant \frac{1}{\varepsilon_2}\left(\frac{m_{11}}{m_{22}}\right)^2|u|^2|\psi_e|^2 + \varepsilon_2 c_r^2|z_v|^2, \tag{62}$$

$$z_v z_r \leqslant \frac{1}{4\varepsilon_3}|z_v|^2 + \varepsilon_3|z_r|^2. \tag{63}$$

Next, we expand and manipulate the fourth term $z_v\delta_v$ in a similar way:

$$\begin{aligned} z_v\delta_v = {} & \frac{m_{11}}{m_{22}}r_R(k+k_1)\left(x_e\cos\psi + y_e\sin\psi\right)z_v \\ & + \left[(k+k_1) - \frac{Y_v}{m_{22}}\right]v_e z_v \\ & - \left(\dot{v}_R + \frac{m_{11}}{m_{22}}u_R r_R + \frac{Y_v}{m_{22}}v_R\right)z_v \\ & - \frac{Y_{v|v|}}{m_{22}}v|v|z_v - (k+k_1) \\ & \cdot (v_R\cos\psi_e - u_R\sin\psi_e - v_R)z_v. \end{aligned} \tag{64}$$

Then, we bound the first three terms of Eq. (64) as follows:

$$\begin{aligned} & \frac{m_{11}}{m_{22}}r_R(k+k_1)(x_e\cos\psi + y_e\sin\psi)z_v \\ & \leqslant \frac{1}{4\varepsilon_4}(k+k_1)^2|r_R|^2|x_e|^2 + \varepsilon_4\left(\frac{m_{11}}{m_{22}}\right)^2|z_v|^2 \\ & \quad + \frac{1}{4\varepsilon_4}(k+k_1)^2|r_R|^2|y_e|^2 + \varepsilon_4\left(\frac{m_{11}}{m_{22}}\right)^2|z_v|^2, \end{aligned} \tag{65}$$

$$\begin{aligned} \left[(k+k_1) - \frac{Y_v}{m_{22}}\right]v_e z_v \leqslant {} & \frac{1}{4\varepsilon_5}\left|\left[(k+k_1) - \frac{Y_v}{m_{22}}\right]\right|^2 \\ & \times|v_e|^2 + \varepsilon_5|z_v|^2, \end{aligned} \tag{66}$$

$$-\left(\dot{v}_R + \frac{m_{11}}{m_{22}}u_R r_R + \frac{Y_v}{m_{22}}v_R\right)z_v \leqslant \frac{1}{4\varepsilon_6}|z_v|^2 + \varepsilon_6|\xi_1|^2, \tag{67}$$

where we have set $\xi_1 = -\dot{v}_R - (m_{11}/m_{22})u_R r_R - (Y_v/m_{22})v_R$. This is a very small quantity since when $\dot{v}_R$ increases $-(m_{11}/m_{22})u_R r_R - (Y_v/m_{22})v_R$ decreases, and they almost cancel each other, see Eq. (2b). For the last two terms in Eq. (64), the following two inequalities hold:

$$-\frac{Y_{v|v|}}{m_{22}}v|v|z_v \leqslant \frac{Y_{v|v|}}{m_{22}}v^2|z_v| \leqslant \frac{1}{4\varepsilon_7}|z_v|^2 + \varepsilon_7\left(\frac{Y_{v|v|}}{m_{22}}\right)^2 v^4, \tag{68}$$

$$\begin{aligned} & -(k+k_1)(v_R\cos\psi_e - u_R\sin\psi_e - v_R)z_v \\ & \leqslant \frac{1}{4\varepsilon_8}|z_v|^2 + \varepsilon_8(k+k_1)^2\xi_2^2, \end{aligned} \tag{69}$$

where we have set the constant $\xi_2 \geqslant |v_R\cos\psi_e - u_R\sin\psi_e - v_R|$; ξ_2 is very small since ψ_e is close to zero during the controlled motion. Also, the quantities r_R^2 and v^4 are very small for the usual operating conditions of an AUV. To proceed further, we consider maximum values for the time-varying quantities that enter the derivative $\dot{V}_4$. Hence, considering the positive constant quantities δ_{max}, u_{max}, $r_{R,max}$, $v_{e,max}$, and v_{max}, it is

$$\delta_1^2 + \delta_2^2 = \|\boldsymbol{\delta}\|^2 \leqslant \delta_{max}^2, \tag{70}$$

$$|u|^2 \leqslant u_{max}^2, \tag{71}$$

$$|r_R|^2 \leqslant r_{R,max}^2, \tag{72}$$

$$|v_e|^2 \leqslant v_{e,max}^2, \tag{73}$$

$$|v|^4 \leqslant v_{max}^4. \tag{74}$$

Then, taking into account the results from Eqs. (61) to (74), Eq. (58) becomes

$$\begin{aligned} \dot{V}_4 = {} & -\left[k - \frac{1}{4\varepsilon_1} - \frac{1}{4\varepsilon_4}(k+k_1)^2 r_{R,max}^2\right]x_e^2 \\ & - \left[k - \frac{1}{4\varepsilon_1} - \frac{1}{4\varepsilon_4}(k+k_1)^2 r_{R,max}^2\right]y_e^2 \\ & - k_1\left(x_e - \frac{\delta_1}{2k_1}\right)^2 - k_1\left(y_e - \frac{\delta_2}{2k_1}\right)^2 \\ & - c_u z_u^2 - c_{3u} z_u^4 - c_r\left(\frac{m_{11}}{m_{22}}u_{max}^2\right)^2 z_v^2 \\ & - \left[c_r - \frac{1}{\varepsilon_2}\left(\frac{m_{11}}{m_{22}}\right)^2 u_{max}^2\right]\psi_e^2 - [c - \varepsilon_3]z_r^2 - c_3 z_r^4 \\ & - \left[c_4 z_u^2 - 2\varepsilon_1 - \varepsilon_2 c_r^2 - \frac{1}{4\varepsilon_3} - 2\varepsilon_4\left(\frac{m_{11}}{m_{22}}\right)^2\right. \\ & \left. -\varepsilon_5 - \frac{1}{4\varepsilon_6} - \frac{1}{4\varepsilon_7} - \frac{1}{4\varepsilon_8}\right]z_v^2 \\ & \cdot \frac{1}{4\varepsilon_5}\left|\left[(k+k_1) - \frac{Y_v}{m_{22}}\right]\right|^2 v_{e,max}^2 + \varepsilon_6|\xi_1|^2 \\ & + \varepsilon_7\left(\frac{Y_{v|v|}}{m_{22}}\right)^2 v_{max}^4 + \varepsilon_8(k+k_1)^2\xi_2^2 + \frac{\delta_{max}^2}{4k_1}. \end{aligned} \tag{75}$$

In Eq. (75), the term $[c_4 z_u^2 - 2\varepsilon_1 - \varepsilon_2 c_r^2 - (\frac{1}{4}\varepsilon_3) - 2\varepsilon_4(m_{11}/m_{22})^2 - \varepsilon_5 - (\frac{1}{4}\varepsilon_6) - (\frac{1}{4}\varepsilon_7) - (\frac{1}{4}\varepsilon_8)]$ must be positive. Setting

$$\begin{aligned} \varepsilon = {} & 2\varepsilon_1 + \varepsilon_2 c_r^2 + \frac{1}{4\varepsilon_3} + 2\varepsilon_4\left(\frac{m_{11}}{m_{22}}\right)^2 \\ & + \varepsilon_5 + \frac{1}{4\varepsilon_6} + \frac{1}{4\varepsilon_7} + \frac{1}{4\varepsilon_8} > 0 \end{aligned} \tag{76}$$

it must be

$$c_4 z_u^2 > \varepsilon \Rightarrow |z_u| > \sqrt{\frac{\varepsilon}{c_4}} \tag{77}$$

which holds for large and positive c_4 and small ε. When $|z_u|$ reaches some small value below $\sqrt{\varepsilon/c_4}$, the terms in the final $\dot{V}_4$ become more negative forcing $|z_u|$ above $\sqrt{\varepsilon/c_4}$ again. Choosing the various gains in order for the coefficients of the states of the error dynamics to be

negative we rewrite Eq. (75) as follows:

$$\begin{aligned}\dot{V}_4 \leqslant & -\kappa_1 x_e^2 - \kappa_1 y_e^2 \\ & - k_1\left(x_e - \frac{\delta_1}{2k_1}\right)^2 - k_1\left(y_e - \frac{\delta_2}{2k_1}\right)^2 \\ & - c_u z_u^2 - c_{3u} z_u^4 - \kappa_2 z_\upsilon^2 \\ & - \kappa_3 \psi_e^2 - \kappa_4 z_r^2 - c_3 z_r^4 - [c_4 z_u^2 - \varepsilon] z_\upsilon^2 + \mu, \end{aligned} \tag{78}$$

where

$$\kappa_1 = \left[k - \frac{1}{4\varepsilon_1} - \frac{1}{4\varepsilon_4}(k+k_1)^2 r_{R,\max}^2\right], \tag{79a}$$

$$\kappa_2 = c_r\left(\frac{m_{11}}{m_{22}} u_{\max}^2\right)^2, \tag{79b}$$

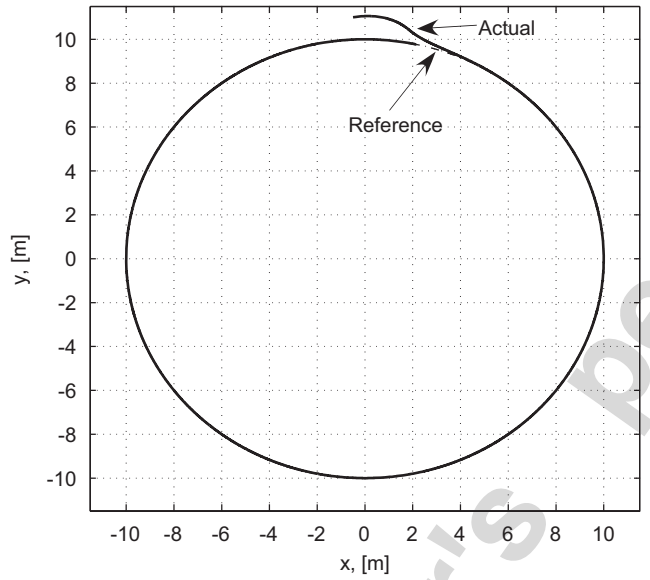

Fig. 4. Circular trajectory tracking. AUV reference and actual path.

$$\kappa_3 = \left[c_r - \frac{1}{\varepsilon_2}\left(\frac{m_{11}}{m_{22}}\right)^2 u_{\max}^2\right], \tag{79c}$$

$$\kappa_4 = [c - \varepsilon_3], \tag{79d}$$

$$\begin{aligned}\mu = & \frac{1}{4\varepsilon_5}\left\|\left[(k+k_1) - \frac{Y_\upsilon}{m_{22}}\right]\right\|^2 \upsilon_{e,\max}^2 + \varepsilon_6|\xi_1|^2 \\ & + \varepsilon_7\left(\frac{Y_{\upsilon|\upsilon|}}{m_{22}}\right)^2 \upsilon_{\max}^4 + \varepsilon_8(k+k_1)^2\xi_2^2 + \frac{\delta_{\max}^2}{4k_1}\end{aligned} \tag{79e}$$

which are all positive. From Eq. (78) it is:

$$\begin{aligned}\dot{V}_4 \leqslant & -\kappa_1 x_e^2 - \kappa_1 y_e^2 - c_u z_u^2 \\ & - \kappa_2 z_\upsilon^2 - \kappa_3 \psi_e^2 - \kappa_4 z_r^2 + \mu. \end{aligned} \tag{80}$$

Also, the final controlled system is represented by the following differential equations:

$$\begin{aligned}\dot{\mathbf{x}}_e = & -\mathbf{K}\mathbf{x}_e - \mathbf{K}_1\mathbf{x}_e + \mathbf{R}\mathbf{z}_u + \boldsymbol{\delta}, \\ \dot{z}_u = & -c_u z_u - c_{3u} z_u^3 - (x_e\cos\psi + y_e\sin\psi) \\ & + \frac{m_{11}}{m_{22}} r_R z_\upsilon - c_4 z_u z_\upsilon^2, \\ \dot{z}_\upsilon = & -c_r\left(\frac{m_{11}}{m_{22}}u\right)^2 z_\upsilon + c_r\left(\frac{m_{11}}{m_{22}}u\right)\psi_e \\ & - \left(\frac{m_{11}}{m_{22}}u\right) z_r - \frac{m_{11}}{m_{22}} r_R z_u + \delta_\upsilon, \\ \dot{\psi}_e = & c_r\frac{m_{11}}{m_{22}} u z_\upsilon - c_r\psi_e + z_r, \\ \dot{z}_r = & -c z_r - c_3 z_r^3 - \psi_e + \left(\frac{m_{11}}{m_{22}}u - 1\right) z_\upsilon. \end{aligned} \tag{81}$$

If we define $\mathbf{z} = [x_e, y_e, \psi_e, z_u, z_\upsilon, z_r]^T$, then, considering Eq. (55) it is $2V_4 = \|\mathbf{z}\|^2$. Taking $\gamma = \min\{\kappa_1, \kappa_2, \kappa_3, \kappa_4, c_u\}$, it is $\dot{V}_4 \leqslant -2\gamma V_4 + \mu$ which, employing the Comparison Lemma (Khalil, 1996), yields $V_4(t) \leqslant V_4(0)\,e^{-2\gamma t} + (\mu/2\gamma)$ for $t \in [0, t_{\text{final}})$. Doing the algebra, we conclude that

$$\|\mathbf{z}(t)\| \leqslant \|\mathbf{z}(0)\| e^{-\gamma t} + \sqrt{\frac{\mu}{\gamma}}, \quad t \in [0, t_{\text{final}}). \tag{82}$$

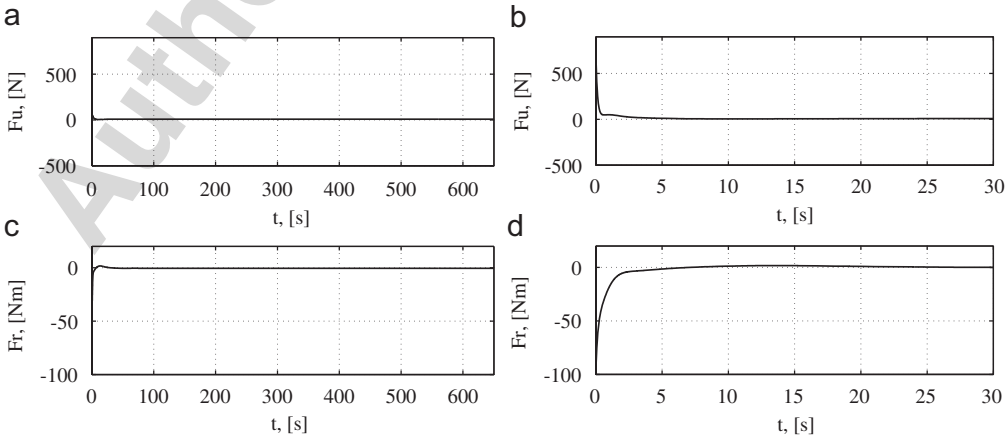

Fig. 5. (a), (c) Control surge force and yaw torque. (b), (d) First 30 s.

Eq. (82) means that the states of the error dynamics remain in a bounded set around zero, which can be reduced by increasing the gains in Eq. (80). At this result we arrived using the controls in Eq. (28) along with Eqs. (59) and (42) and (57).

5. Simulations

A number of simulation results showed that the above designed controller performs very well in terms of quick convergence of the tracking errors to a small neighborhood of zero, smooth transient responses, low control effort, and robustness in the case of large initial errors or when the designer has no accurate knowledge of the model parameters. To illustrate the performance of the proposed trajectory planning and tracking control methods, typical simulation results are presented. In all of the following simulations we applied the same controller structure for the force F_u and the torque F_r using the same values for the

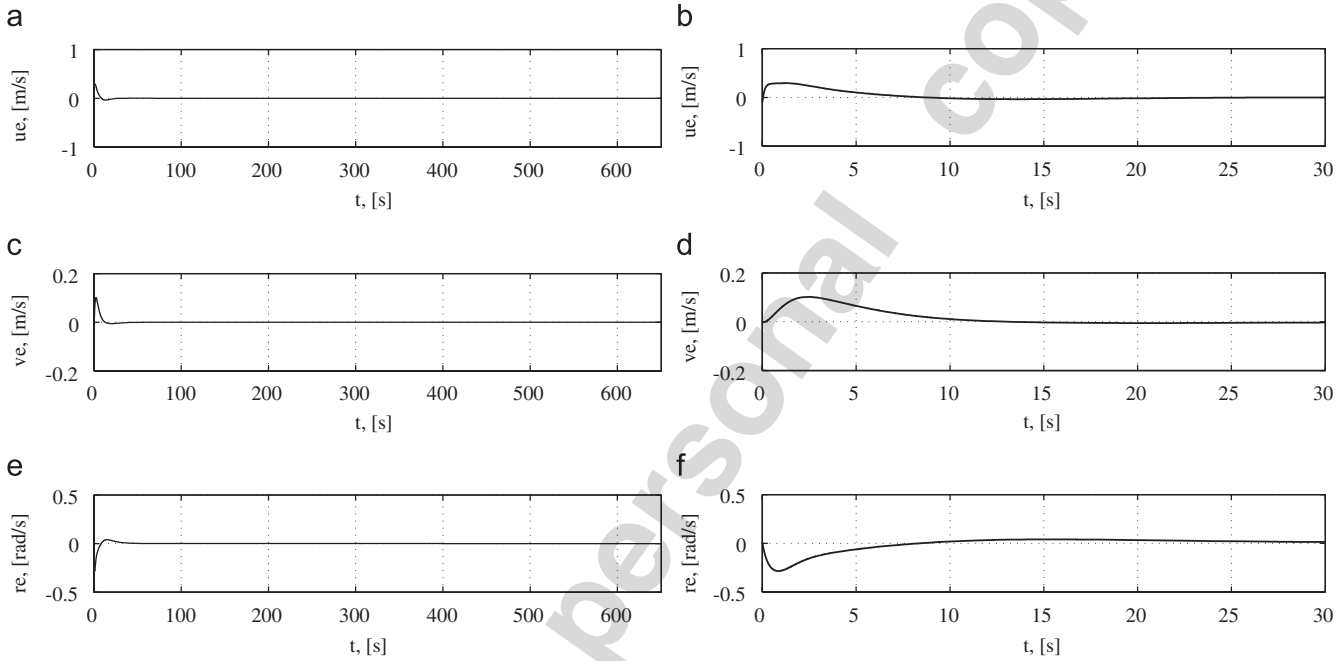

Fig. 6. (a), (c) Linear velocity tracking errors. (b), (d) First 30 s. (e) Angular velocity tracking error. (f) First 30 s.

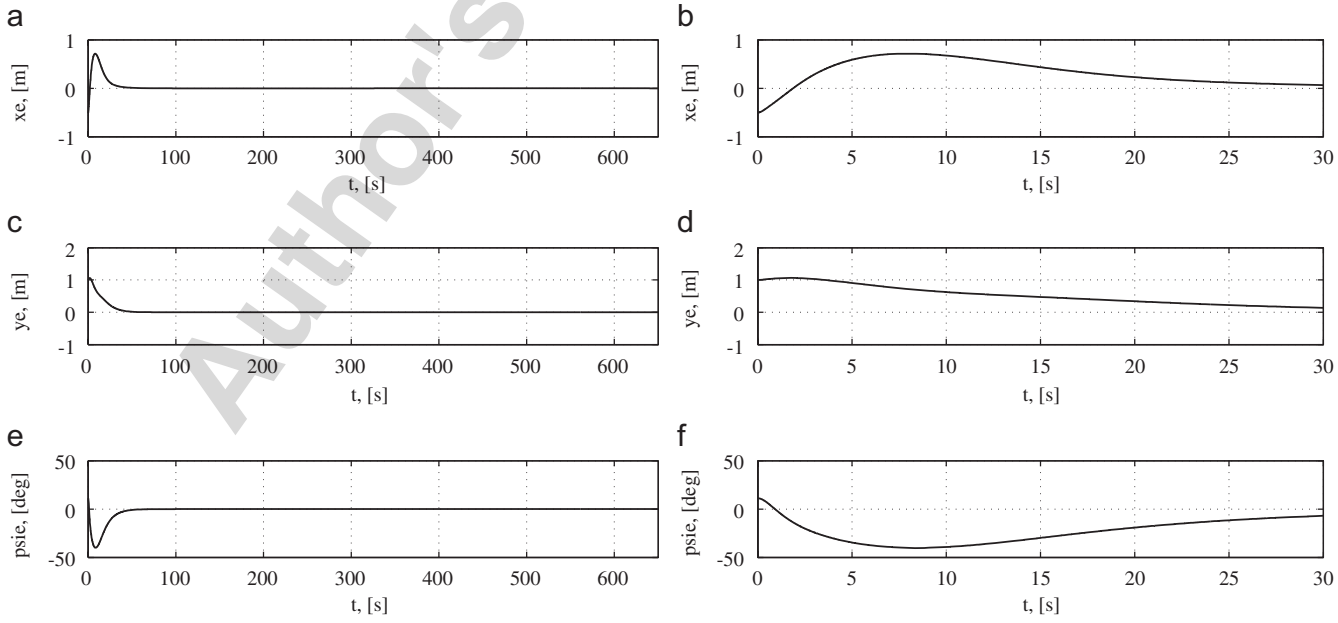

Fig. 7. (a), (c) Position tracking errors. (b), (d) First 30 s. (e) Orientation tracking error. (f) First 30 s.

various gains that enter into the controller equations; that is, the closed-loop control design is independent of the trajectory to be tracked. Specifically, we used the gains $k = 0.5$, $k_1 = 0.4$, $c_u = 2$, $c_{3u} = 3$, $c_4 = 3$, $c_5 = 3$, $c_r = 0.1$, $c = 2$, and $c_3 = 1$. They are the result of a compromise between the need of negative coefficients of the states in the derivative of V_4, the need of small magnitude for the nonnegative terms in $\dot{V}_4$, and the need for smooth control efforts, so that they can be produced by real vehicle actuators.

The desired trajectories, for which closed-loop tracking control simulations are presented, are the circular and the sinusoidal path used for trajectory planning and open-loop control design in Section 3. Responses were obtained for two cases: (a) when the model parameters are known and (b) when there are inaccuracies of the order of 5% in all vehicle parameters.

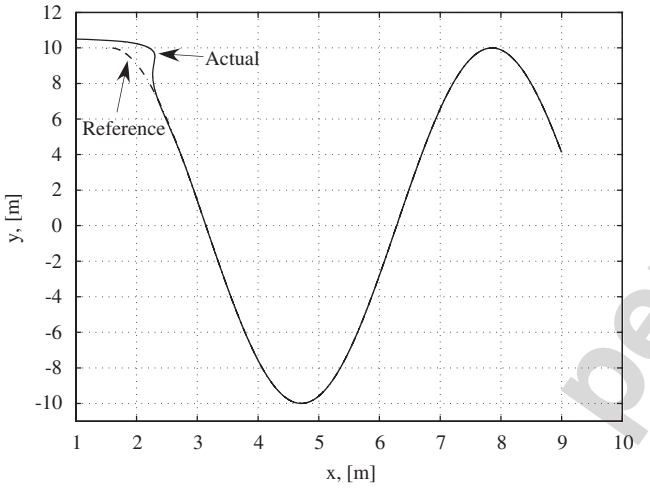

Fig. 8. Sinus trajectory tracking. AUV reference and actual path.

5.1. Circle tracking with accurate model

The following simulations concern the trajectory planning and tracking control design for a circular path in Section 3.3, based on the accurate knowledge of the model parameters. Here, the AUV starts from rest, resulting in initial velocity errors of $|u_e| = 0.1$ m/s, $|v_e| = 0.0021$ m/s, and $|r_e| = 0.01$ rad/s, and initial position and orientation errors of $|x_e| = 0.5$ m, $|y_e| = 1$ m, and $|\psi_e| = 30^\circ$. In Fig. 4, the reference and the resulting trajectory, under the action of the controller, of the CM of the vehicle in the inertial X–Y plane are displayed. Fig. 5 shows the control force F_u and the control torque F_r needed for tracking. After a short period of time—needed for the errors to converge to a small neighborhood of zero—they converge smoothly, see on the right of Fig. 5 where the first 30 s are displayed, to their open-loop values given by Eqs. (20) and (21). The errors in velocities are depicted in Fig. 6. The figures on the left regard a simulation time of 650 s—needed for one full circle—while the figures on the right the first 30 s, in order to observe the transient response. We see that after a short time period, they converge to a very small neighborhood of zero, of the order of 10^{-5} m/s or rad/s, and slowly oscillate within. The errors in position and orientation are shown in Fig. 7. The figures on the left regard a simulation time of 650 s while the figures on the right the first 30 s. Again, after a smooth transition period the errors converge and remain to a small neighborhood of zero of the order of 10^{-5} m or deg.

5.2. Sinus tracking with accurate model

Here, the controller has to deal with time-varying velocities with relatively large magnitudes. This leads to time-varying nonlinear dynamical couplings, see Eqs. (1) and (2) as well as Eqs. (26) and (27). Consider also Fig. 3,

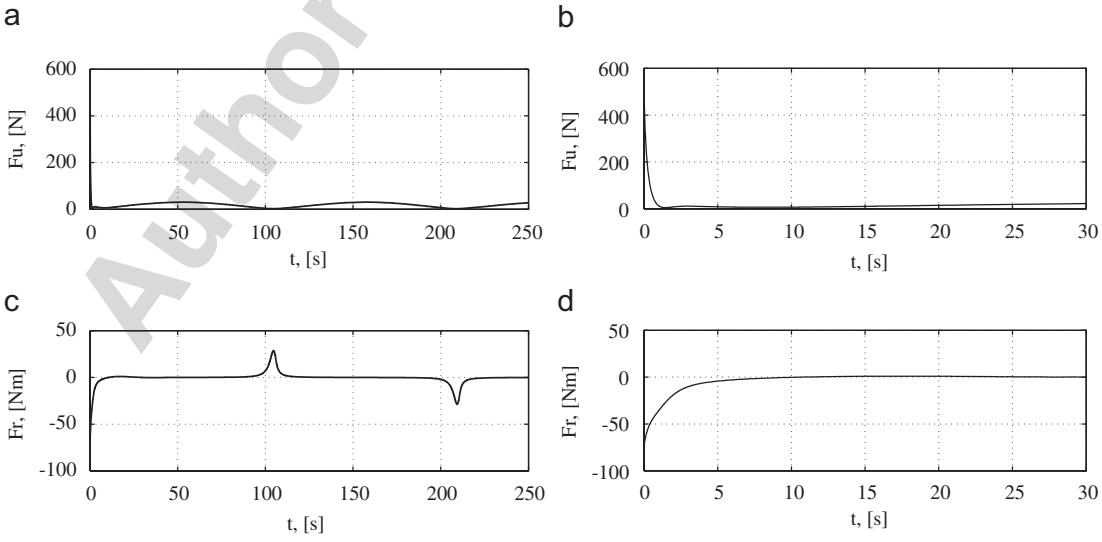

Fig. 9. (a), (c) Control surge force and yaw torque. (b), (d) First 30 s.

where one can also observe the change of the orientation of the AUV relative to the path. The vehicle starts from rest, resulting in initial velocity errors of $|u_e| = 0.03$ m/s, $|v_e| = 0.017$ m/s, and $|r_e| = 0.32$ rad/s, and initial position and orientation errors of $|x_e| = 0.5$ m, $|y_e| = 0.5$ m, and $|\psi_e| = 0.2^\circ$. In Fig. 8, the reference and the resulting trajectory of the CM of the vehicle in the inertial X–Y plane are displayed. Fig. 9 shows the control force F_u and the control torque F_r needed for tracking. After a relatively small time interval—needed for the errors to converge to a small neighborhood of zero—they converge smoothly to their open-loop time-varying values, see on the right of

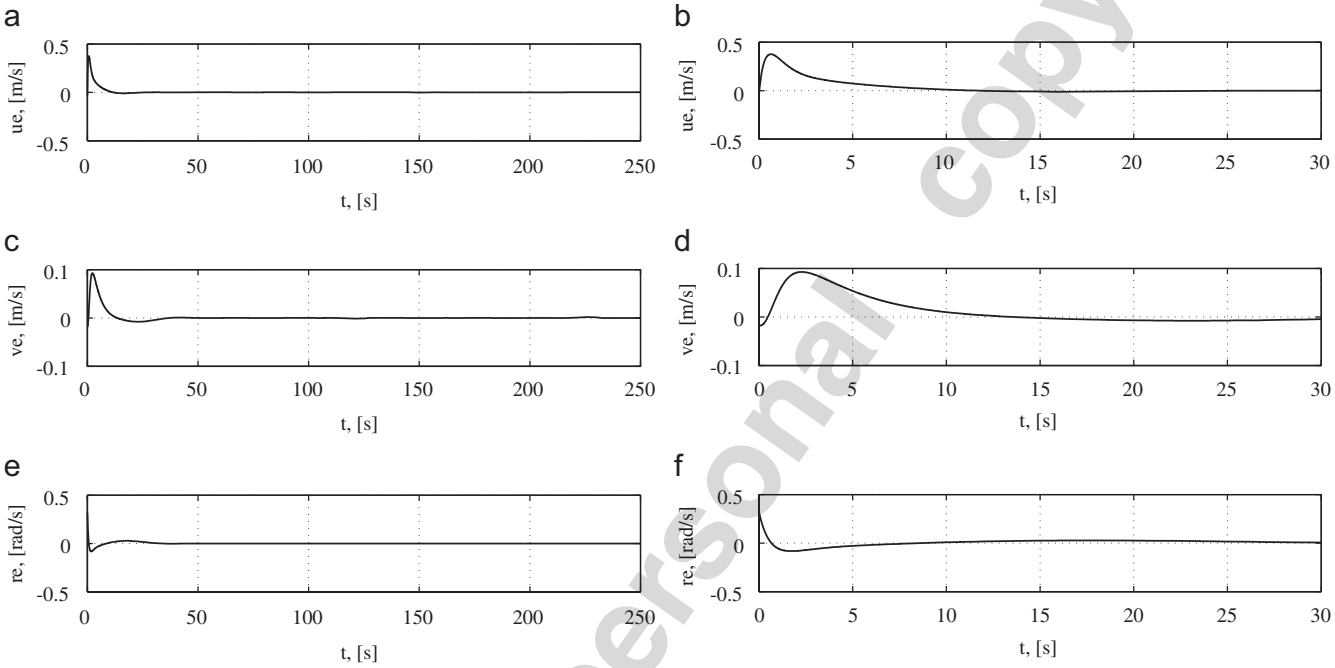

Fig. 10. (a), (c) Linear velocity tracking errors. (b), (d) First 30 s. (e) Angular velocity tracking error. (f) First 30 s.

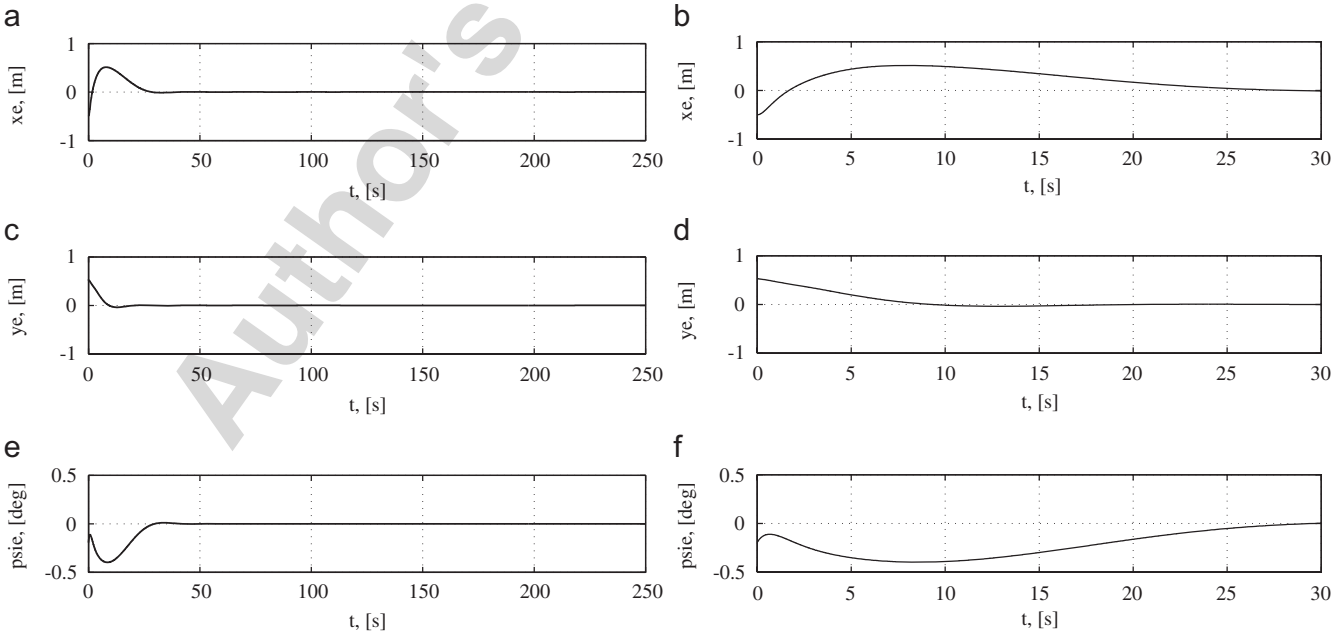

Fig. 11. (a), (c) Position tracking errors. (b), (d) First 30 s. (e) Orientation tracking error. (f) First 30 s.

Fig. 9 where the first 30 s are depicted. These control efforts are larger with respect to the previous circular tracking—given by Eqs. (20) and (21). The errors in velocities are depicted in Fig. 10. The figures on the left regard a simulation time of 250 s—needed for one full period for the sinus function—while the figures on the right the first 30 s. Hence, we see that after a relatively small time period, they converge to a very small neighborhood of zero, of the order of 10^{-3} m/s or rad/s, and slowly oscillate within. The tracking errors in position and orientation are shown in Fig. 11. We observe that after a smooth transition period the errors converge and remain to a small neighborhood of zero of the order of 10^{-5} m or deg.

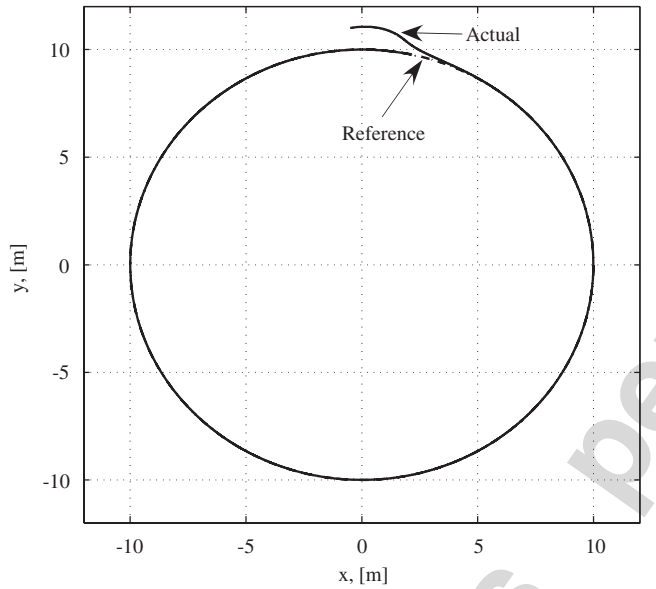

Fig. 12. Circular trajectory tracking. AUV reference and actual path.

5.3. Circle tracking with 5% error in system parameters

In this, and in the subsequent section, we present some results concerning the robustness properties of the designed trajectory-tracking scheme to model parametric uncertainty. Specifically, we conducted simulations in which errors of the order of 5% on all parameters in Table 1 were assumed. The initial conditions are the same as in Section 5.1. In Fig. 12, the reference and the resulting trajectory, under the action of the controller, of the CM of the vehicle in the inertial X–Y plane are displayed. Fig. 13 shows the control force F_u and the control torque F_r needed for tracking. Contrary to the fact that there are errors mainly in the feedforward part of the controller, the feedback part—although there are also modeling errors here—corrects the motion of the vehicle, guides the errors of the states to a small neighborhood of zero and compensates for the errors in the model parameters as well. The errors in velocities are depicted in Fig. 14. The figures on the left regard a simulation time of 650 s while the figures on the right the first 30 s. They converge to a very small neighborhood of zero, of the order of 10^{-4} m/s or rad/s, and slowly oscillate within. The tracking errors in position and orientation are shown in Fig. 15. They also converge and remain to small neighborhood of zero of the order of 10^{-4} m or deg.

5.4. Sinus tracking with 5% error in system parameters

Finally, simulations regarding trajectory tracking of the fast—regarding the magnitudes of the reference velocities—sinusoidal path are presented considering errors of the order of 5% on all system parameters. The initial conditions are the same as in Section 5.2. In Fig. 16, the reference and the resulting trajectory are displayed. Fig. 17 shows the control force F_u and the control torque F_r needed for tracking; again the feedback part of the controller

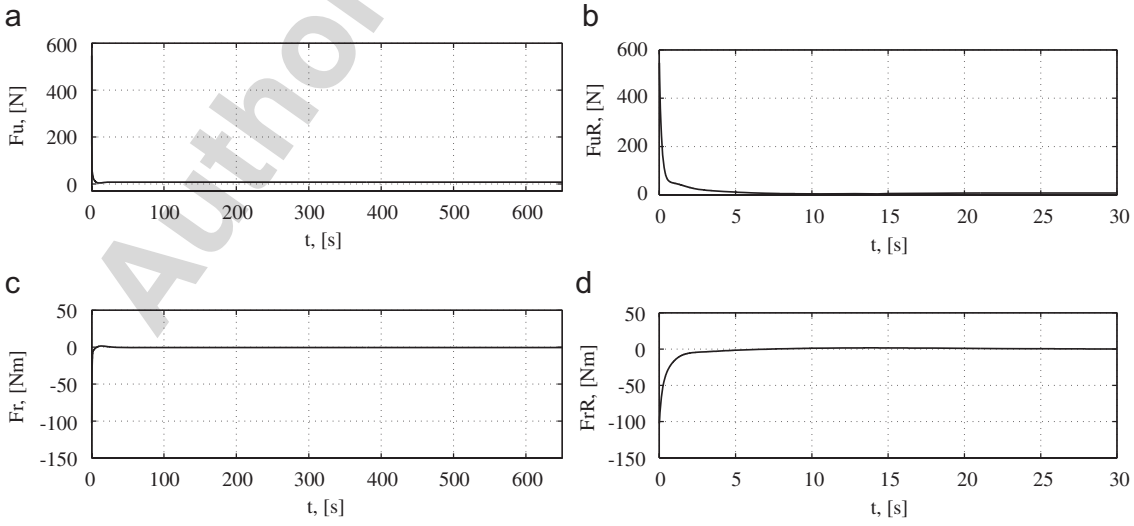

Fig. 13. (a), (c) Control surge force and yaw torque. (b), (d) First 30 s.

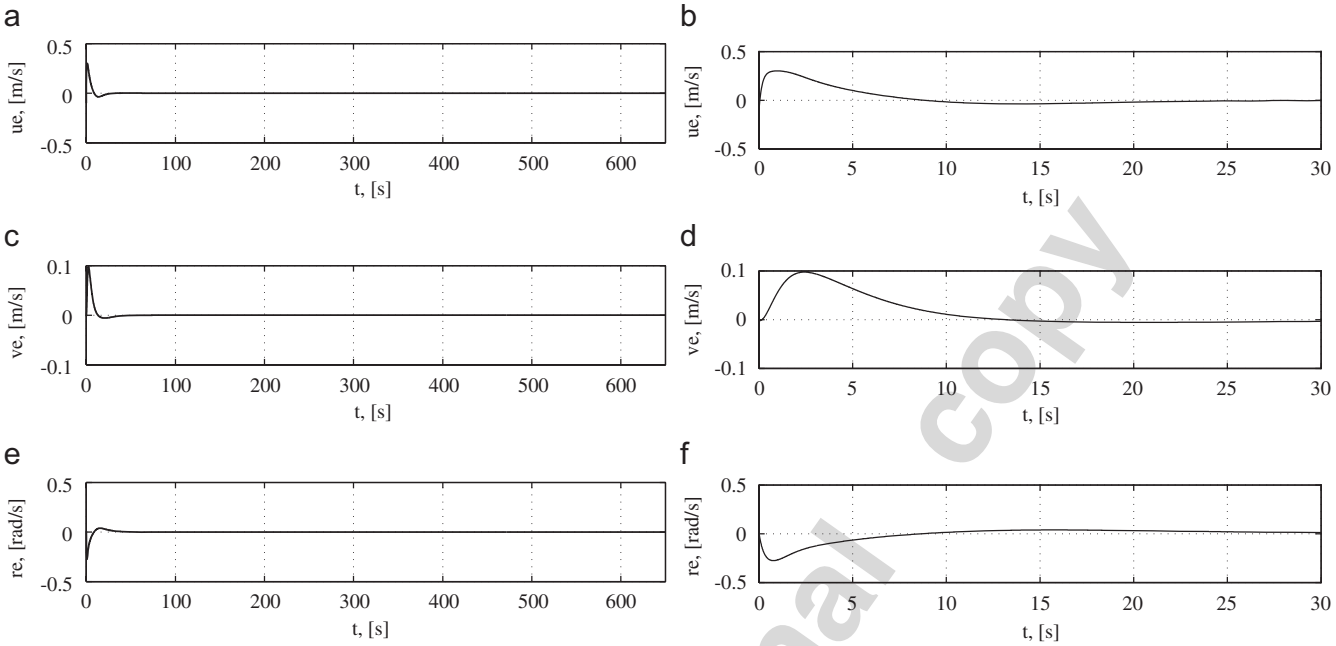

Fig. 14. (a), (c) Linear velocity tracking errors. (b), (d) First 30 s. (e) Angular velocity tracking error. (f) First 30 s.

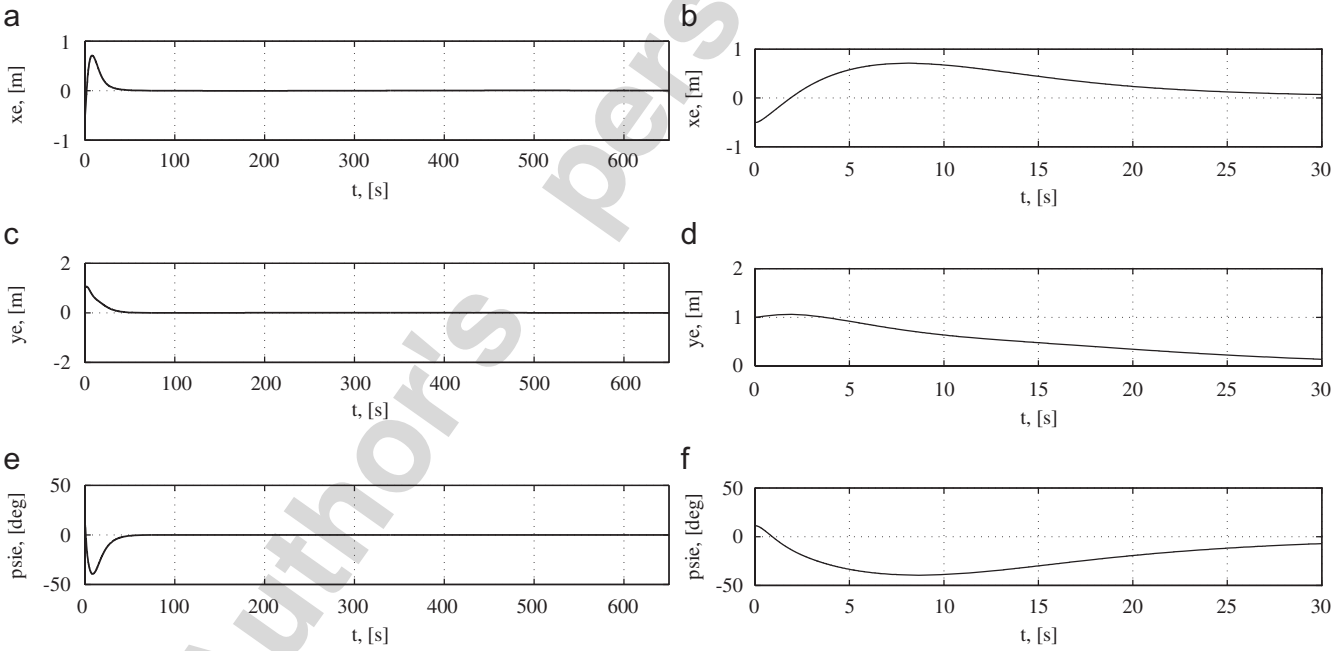

Fig. 15. (a), (c) Position tracking errors. (b), (d) First 30 s. (e) Orientation tracking error. (f) First 30 s.

undertakes the effort to compensate for the errors in the states and in model parameters. The errors in velocities, in positions, and orientation, are depicted in Figs. 18 and 19, respectively. In this case, the effects of underactuation—see for example υ_e response—, and of large nonlinear dynamical couplings and parameter errors that affecting the sign of $\dot{V}_4$ are evident. The structure of the closed-loop controller, however, keeps the errors in a fairly small neighborhood close to zero.

6. Conclusions

In this paper, the combined problem of trajectory planning and tracking control for underactuated AUVs

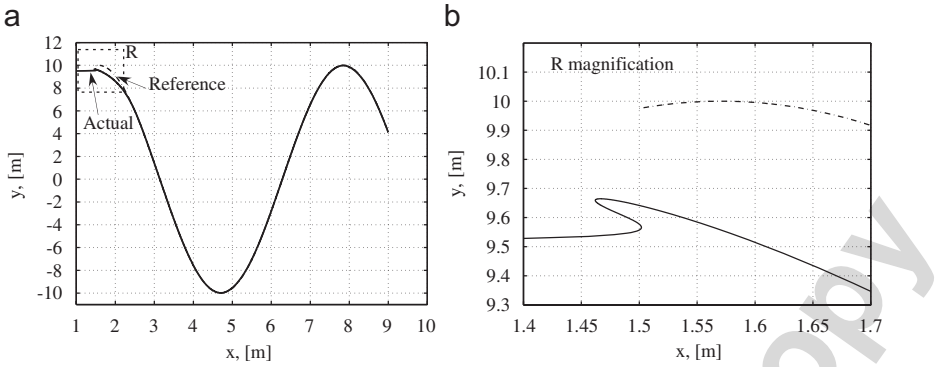

Fig. 16. (a) Sinus trajectory tracking. AUV reference and actual path. (b) First 30 s.

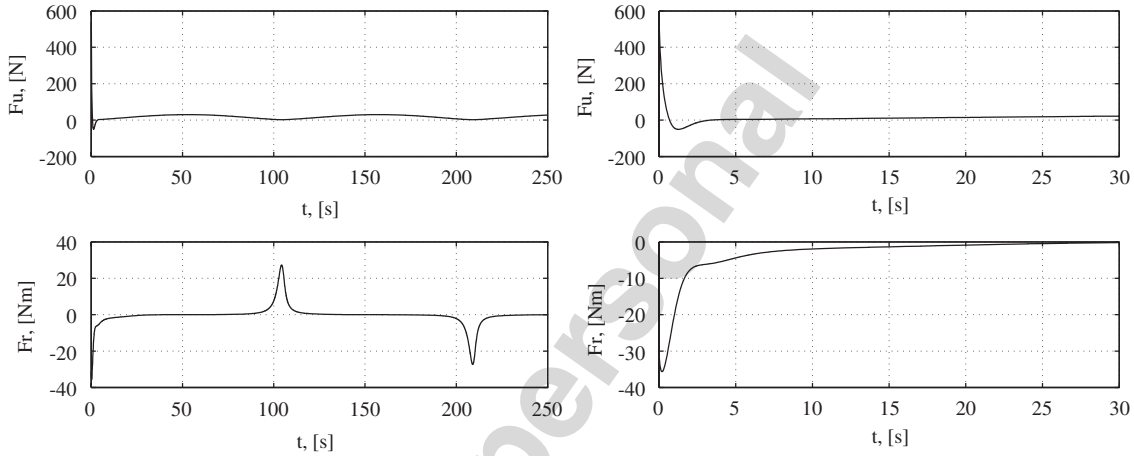

Fig. 17. (a), (c) Control surge force and yaw torque. (b), (d) First 30 s.

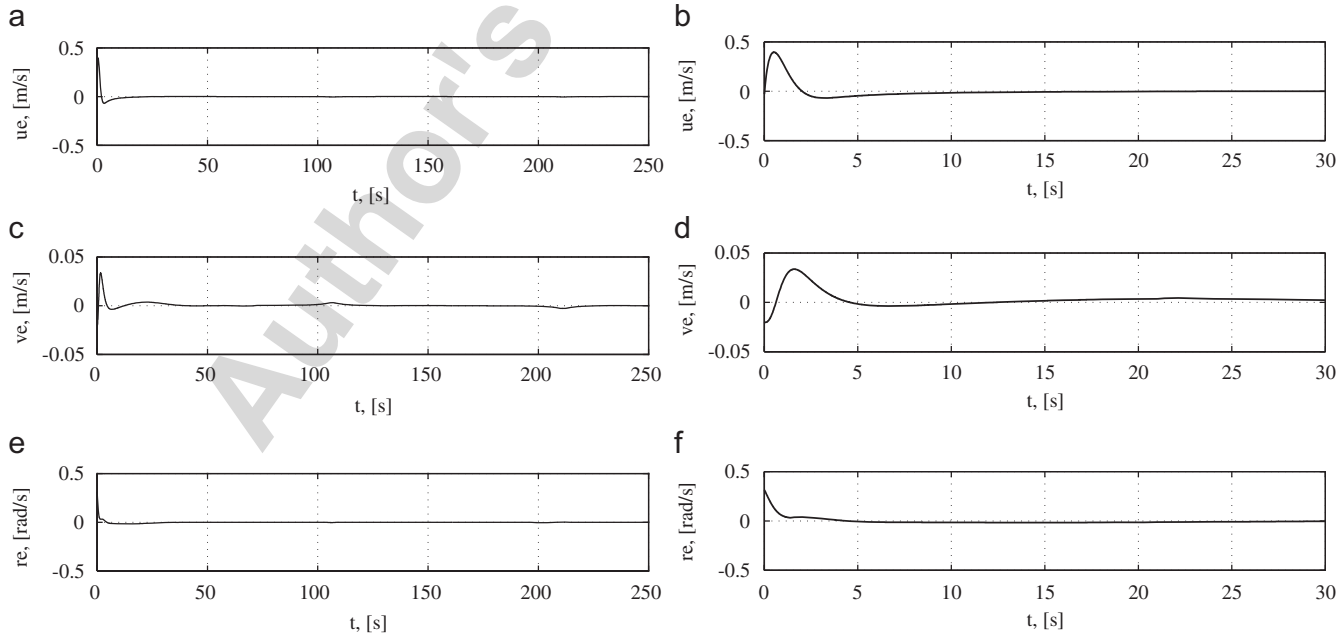

Fig. 18. (a), (c) Linear velocity tracking errors. (b), (d) First 30 s. (e) Angular velocity tracking error. (f) First 30 s.

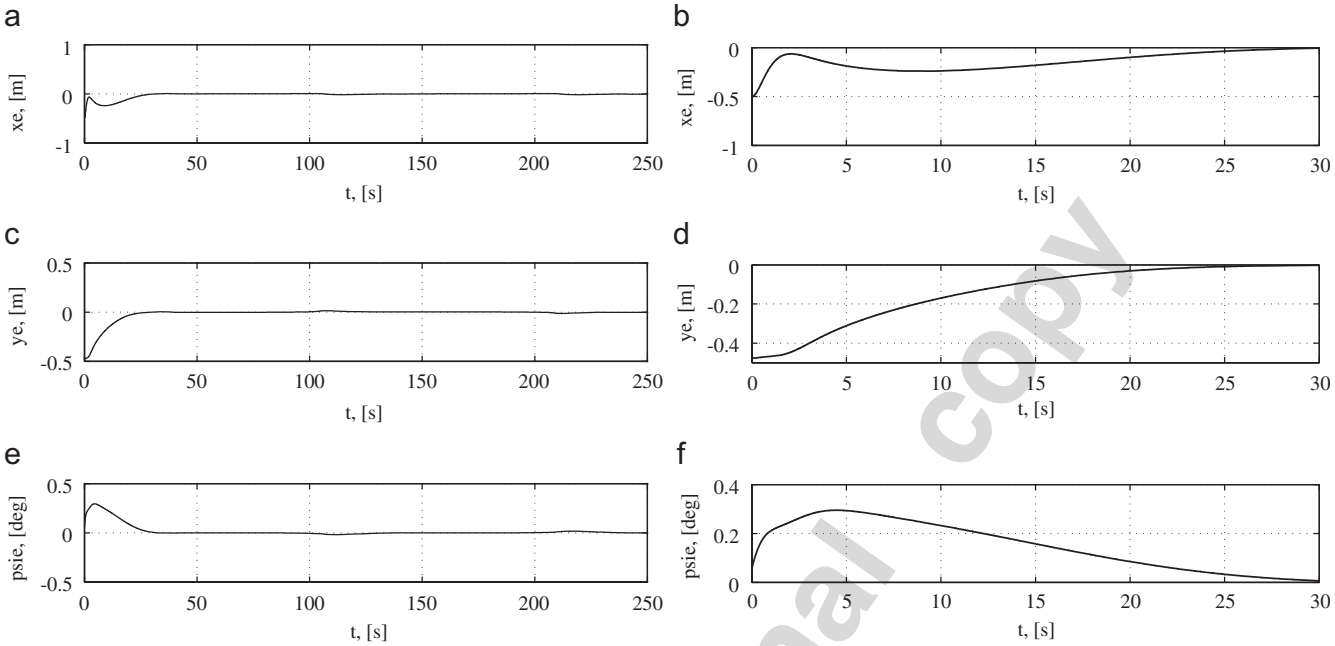

Fig. 19. (a), (c) Position tracking errors. (b), (d) First 30 s. (e) Orientation tracking error. (f) First 30 s.

moving on the horizontal plane was addressed. Given a reference, smooth, inertial 2D trajectory to be followed by the vehicle CM, the planning algorithm uses the vehicle dynamic model, and yields the corresponding body-fixed linear and angular velocities as well as the vehicle's orientation. Using these reference values, the dynamics of the AUV was transformed to the error one. Backstepping techniques were utilized to stabilize the above system and force the tracking error to a neighborhood about zero that can be made arbitrarily small. Computer simulations showed very good tracking performance and robustness of the proposed method in the presence of parametric uncertainty or of trajectories that are described by time-varying velocities.

References

Aguiar, P.A., Hespanha, J.P., 2003. Position tracking of underactuated vehicles. In: Proceedings of the 2003 American Control Conference, ACC 03, Denver, CO, USA.

Aguiar, A.P., Pascoal, A.M., 2002. Dynamic positioning and way-point tracking of underactuated AUVs in the presence of ocean currents. In: Proceedings of the 41st IEEE Conference on Decision and Control, CDC 02, Las Vegas, Nevada, USA, pp. 2105–2110.

Behal, A., Dawson, D.M., Dixon, W.E., Fang, Y., 2002. Tracking and regulation control of an underactuated surface vessel with nonintegrable dynamics. IEEE Transactions on Automatic Control 47 (3), 495–500.

Fossen, T.I., 1994. Guidance and Control of Ocean Vehicles. Wiley, New York.

Jiang, Z.P., 2002. Global tracking control of underactuated ships by Lyapunov's direct method. Automatica 38 (1), 301–309.

Kaminer, I., Pascoal, A., Hallberg, E., Silvestre, C., 1998. Trajectory tracking for autonomous vehicles: an integrated approach to guidance and control. Journal Guidance, Control and Dynamics 21 (1), 29–38.

Khalil, H.K., 1996. Nonlinear Systems, second ed. Prentice-Hall, Upper Saddle River.

Krstic, M., Kanellakopoulos, I., Kokotovic, P., 1995. Nonlinear and Adaptive Control Design. Wiley, New York.

Lefeber, E., Pettersen, K.Y., Nijmeijer, H., 2003. Tracking control of an underactuated ship. IEEE Transactions on Control Systems Technology 11 (1), 52–61.

Mazenc, F., Pettersen, K.Y., Nijmeijer, H., 2002. Global uniform asymptotic stabilization of an underactuated surface vessel. IEEE Transactions on Automatic Control 47 (10), 1759–1762.

Pettersen, K.Y., Egeland, O., 1999. Time-varying exponential stabilization of the position and attitude of an underactuated autonomous underwater vehicle. IEEE Transactions on Automatic Control 44 (1), 112–115.

Pettersen, K.Y., Fossen, T.I., 2000. Underactuated dynamic positioning of a ship—experimantal results. IEEE Transactions on Control Systems Technology 8 (5), 856–863.

Pettersen, K.Y., Nijmeijer, H., 2001. Underactuated ship tracking control: theory and experiments. International Journal of Control 74 (14), 1435–1446.

Repoulias, F., Papadopoulos, E., 2005. Trajectory planning and tracking control design of underactuated AUVs. In: Proceedings of the IEEE International Conference on Robotics and Automation, ICRA 05, Barcelona, Spain, pp. 1622–1627.

Reyhanoglou, M., 1997. Exponential stabilization of an underactuated autonomous surface vessel. Automatica 33 (12), 2249–2254.

Wichlund, K.Y., Sordalen, O., Egeland, O., 1995. Control properties of underactuated vehicles. In: Proceedings of the IEEE International Conference on Robotics and Automation, ICRA 95, pp. 2009–2014.

Yuh, J., 2000. Design and control of autonomous underwater robots: a survey, International Journal of Control (8), 7–24.